Chapter 5
Reduction and Analysis of Observational Data: Flux and Transport of Properties

Aspects related to the numerical treatment and analysis of observational data, which were included as items of the project component list (Table 4.1, Chap. 4) necessary to the project development, will be presented in this chapter. This comprises data reduction and analysis of scalar (hydrographic properties and tide) and vector (current velocity) data sampled in the water column (vertical profiles) and/or as temporal time series.

At this stage is important not to characterize the estuarine environment only in terms of its spatial and temporal variation of hydrographic properties and circulation. It is also important to value the theoretical interpretation of results. The hydrographic properties are very important in determining the flux and the transport of volume, concentration of salt, nutrients, pollutants and suspended sediments, and to establish the main characteristics of the importation or exportation of these concentrations. However, they do not provide the full dynamical understanding about the estuary, which is a much large picture.

5.1 Decomposition of Velocity

The magnetic (or electronic) compass inside the velocity measuring device is oriented to the North magnetic field of Earth, and the measured angle indicates the direction and its orientation relative to this magnetic field. As with the estuaries, special attention must be given to the longitudinal and transversal (secondary) velocity components as well as to the decomposition of the velocity vector.

Before considering the decomposition of velocity measured in an estuary, some elementary considerations will be given in relation to a vector denoted by $\vec{v}$, relative to a plane orthogonal reference system (Oxy). According to the reference system in Fig. 2.8 (Chap. 2), the u and v-velocity components in relationship to the Ox and Oy axes are calculated, respectively, as

L. Bruner de Miranda et al., *Fundamentals of Estuarine Physical Oceanography*,
Ocean Engineering & Oceanography 8, DOI 10.1007/978-981-10-3041-3_5

$$u = V\cos(\theta), \tag{5.1}$$

and

$$v = V\sin(\theta). \tag{5.2}$$

In these equations V is the intensity of the velocity vector $(\vec{v})$, and θ is the trigonometric angle formed between the abscissa (Ox), measured in an anti-clock wise rotation. Then, this vector decomposition will result in u and v-velocity components that are positive, negative or null, according to the angle.

If the vector $(\vec{v})$ is the velocity at a given position in the estuary, measured by a current-meter, it has an intensity (V) and a direction denoted by the angle (dd). As the direction of the current velocity is measured in the clockwise rotation, with its origin in the North magnetic field (Fig. 5.1b), and the origins of the angles θ and dd aren't coincidental, it is necessary to answer the following question: how to achieve the decomposition of the vector velocity in the components u and v, with the system of Eqs. (5.1) and (5.2)?

To answer this question, the first thing required is to make the origins of these angles (dd and θ) the same, because the trigonometric Eqs. (5.1) and (5.2), may only be applied for angles with that origin. Secondly, it must be taken into account whether the rotation angle has opposite directions (clockwise and anti-clockwise). In Fig. 5.1a it is possible to verify that these origins will be the same if the trigonometric angle θ is calculated by:

$$\theta = 90^\circ - dd \tag{5.3}$$

Now, it is necessary to adjust the magnetic North (NM) to the true North. This adjustment is of great practical importance when we need to plot the vector velocity in a nautical chart, because they are displayed in relation to the true north. This may be done without difficulty if the local magnetic declination angle (D), which is a deviation of the true North to east or west, is known. Magnetic declination varies

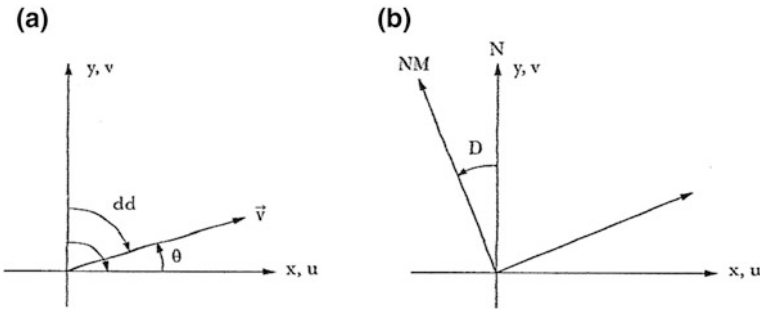

Fig. 5.1 **a** Decomposition of a velocity vector $(\vec{v})$ in an orthogonal reference system; **b** the same velocity vector in relation to the magnetic North (NM) and the true North (N), respectively

both with time and with geographical location due to astronomic and geophysical phenomena. Nautical charts present this angle and its annual variation along with the chart printing date, to enable its extrapolation and correction for the date when the experiment was performed. Thus, to adjust the magnetic direction, dd, to the true North, in the case of a declination to the west (anti-clockwise), as shown schematically in Fig. 5.1b, it is necessary to change the direction angle dd by (dd − D), in Eq. 5.3. If the magnetic declination is to the east (clockwise), the substitution should be made by the angle dd + D. Then, it follows that

$$\theta = 90^\circ - (\underline{dd} \pm D) \tag{5.4}$$

and the signals + and − (between parenthesis) are applied when the magnetic declination is to the east or west, respectively.

Finally, let us consider an estuary with its longitudinal axis oriented according to an angle, γ, in relation to the true North, such as in Fig. 5.2. This angle (γ) corresponds to an anti-clockwise rotation for the Ox axis to be in the longitudinal direction and oriented positively seaward. Thus, for Eqs. 5.1 and 5.2 which are used in this decomposition, the value θ of Eq. 5.4 must be subtracted from the rotation angle (γ); in the case of a clockwise rotation this angle (γ) must be added to the angle (θ). Then, the final angle θ angle for the decomposition of the velocity vector in an estuary is:

$$\theta = 90^\circ - (dd \pm D) \pm \gamma \tag{5.5}$$

Substitution of the angle (θ), into Eqs. (5.1) and (5.2), will enable calculate the velocity components (u and v) which are necessary for estuarine circulation

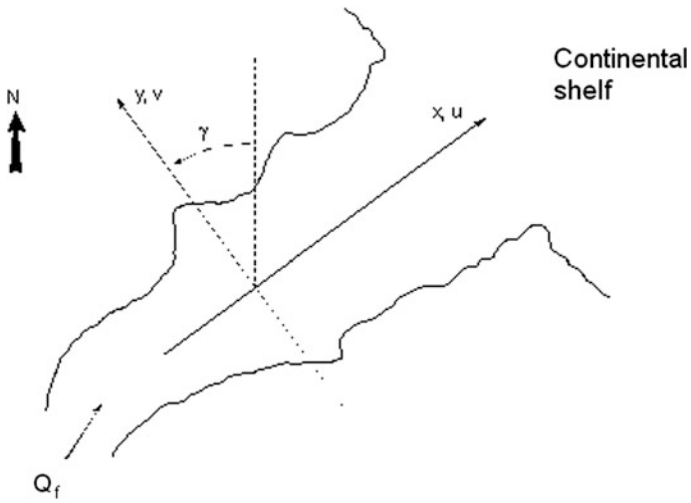

Fig. 5.2 Decomposition of a current velocity vector ($\vec{v}$) into u and v components (longitudinal and transversal, respectively), in relation to the local coordinate system (Oxy)

analysis, and calculation of advective and diffusive transports. According to the longitudinal axis orientation (Fig. 5.2), positive and negative values of the u-velocity component indicates seaward (ebb) and landward (flood) motions, respectively, or, in relation to the tide motions ebb and flood, respectively.

Wind stress is one of the main forces generating the circulation in the oceanic and coastal seas and may influence the circulation and vertical stratification in estuaries (Weisberg 1976; Elliott 1976; Geyer 1997; Valle-Levinson et al. 1998; and others). It is also necessary to calculate the wind-velocity components which are required to determine the correlation of wind stress with current velocity measured on the open sea and in estuaries, to investigate the strength of its influence on the circulation. However, wind velocity measured with an anemograph often refers to the direction in which the wind is coming from. This is the opposite convention to current velocity. Therefore, in such cases it is necessary to rotate the wind velocity by 180° to match the current velocity convention, so that correlation between the wind velocity components (U_v, V_v) and the current velocity components (u, v) can be measured. Then, the wind velocity decomposition can be made with the following set of equations:

$$U_v = U\cos(\vartheta), \tag{5.6}$$

and

$$V_v = U\sin(\vartheta), \tag{5.7}$$

where U indicate the wind intensity and the angle ϑ is given by:

$$\vartheta = 270^\circ - dd_V \pm \gamma, \tag{5.8}$$

with dd_V indicating the wind direction. The 270° angle is 180° out of phase in relation to Eq. (5.4), and the magnetic declinations have not been taken into account because, generally, they usually are compensated during the anemograph installation in coastal meteorological stations. If the wind vector direction is referenced as the current motions at sea, which has also been used in wind measurements, the ϑ angle of Eq. (5.8) must be adjusted to $\vartheta = 90^\circ - dd_V \pm \gamma$.

As an example of decomposition of a velocity vector measured in an estuary, consider the intensity and direction of velocity presented in Table 2.2 (Chap. 2), in the assumption that the estuary is oriented in the north-south direction and that the estuary mouth is located to the south. Then, by rotating the Ox axis 90° clockwise, it will be oriented southward and towards the estuary mouth. At the position of the original measurements, the magnetic declination was 20° towards west (D = 20°), and the final rotation angle is $\theta = 90^\circ - (dd - 20^\circ) + 90^\circ = 180^\circ - (dd - 20^\circ)$. The results obtained by applying Eqs. (5.1) and (5.2) to calculate the vertical profiles of the u and v-velocity components are presented in Table 5.1. This table shows that $|u| \gg |v|$ at times t_1 and t_2; however, in the experiment, at time t_2 (current with low speed near slack water), the signal of the u-component changes

Table 5.1 Longitudinal (u) and transversal (v) velocity components calculated with vector velocities and direction from Table 2.2 (Chap. 2)

Depth (m)	u (m s^{-1}) (t_1)	v (m s^{-1}) (t_1)	u (m s^{-1}) (t_2)	v (m s^{-1}) (t_2)
0.0	1.09	−0.02	0.22	0.01
1.0	1.07	0.23	0.20	0.05
2.0	0.92	0.21	0.10	0.00
3.0	0.84	0.13	−0.02	0.01
4.0	0.74	0.04	−0.19	−0.03
5.0	0.59	0.02	−0.30	−0.02
6.0	0.40	0.19	−0.32	−0.06
7.0	0.26	0.14	−0.47	−0.02

Time measurements on the ebb tide are indicated by t_1 and t_2

direction at 3 m depth from seaward to landward, indicating that this direction change was forced by the intensity increase of the baroclinic component of the gradient pressure force (Eq. 2.10, Chap. 2).

5.2 Vertical Velocity Profiles

Continuous or discrete profile measurements of hydrographic properties and current velocity must be interpolated at discrete depths, usually at equidistant depths between the surface and the bottom. These discrete values may be obtained by graphical or numeric methods of interpolation, the latter being the best for minimizing errors and when the number of profiles is large. Among the numerical methods, we may cite the Lagrange and the *cubic spline*.

In the cubic splines, cubic polynomials are found to approximate the curve between each pair of data points, and the data adjustment is made by a third degree polynomial enabling the interpolations at pre-selected points. In the language of splines, these data points are called the breakpoints, and, since a straight line is uniquely defined by two points, an infinite number of cubic polynomials can be used to approximate a curve between two points. If the discrete profile has N measured quantities from the surface down to the bottom, this method assumes that the extreme polynomial points have no curvature, that is, the second derivative in relation to these points is null, or the curvature is constant. Thus, if the angular coefficient is known, extrapolations may be performed along the water column, from the surface and down to the bottom (Pennington 1970; Hanselman and Littlefield 1998). To obtain best results with this method, two conditions must be satisfied: (i) the experimental measurements must be made as close as possible to the surface and bottom; and (ii) the number of experimental data points must be higher than the number of depths to be interpolated in the water column. Further details on cubic splines processing in MatLab® computational environment may be found in Hanselman and Littlefield (op. cit).

According to the basic principles of hydrodynamics, the stress is proportional to the velocity component perpendicular to the motion, and the maximum friction is related to the water molecules at the bottom solid surface, with no horizontal significant movement. The friction at the bottom is estimated as a function of the velocity, called the *friction velocity* (to be defined in this chapter), or as a function of the amplitude of the tidal velocity and the water column depth. Due to this bottom characteristic, the velocity shear has a distinct structure called *boundary layer*, where the fluid velocity goes to zero or has a small value indicating a no-slip and a slippery bottom conditions, respectively.

Under simplified conditions, the velocity intensity increases from the bottom towards the surface until the motion occurs as if the bottom was a smooth surface (Chriss and Caldwell 1984), as schematically shown in Fig. 5.3a. Assuming this figure illustrates the unidirectional motion in an estuary during the ebb tide, in a later time the flow may be in the opposite direction (tidal flood), or may even be a bidirectional turbulent motion (flood and ebb), because in these coastal environments the circulation can be very complex, and turbulent fluctuations of velocity across the main flow may also occur causing vertical instabilities.

The estuarine water mass circulation has a free surface Newtonian fluid behavior and its intensity decreases with depth due to internal friction and frictional shear stress at the boundaries. The turbulence transmission due to velocity shears in the water column is caused by momentum exchange between layers, which may be parameterized by an eddy viscosity coefficient. As may be observed, near the bottom (which is plane and smooth by hypothesis), the fluctuating velocity profile is gradually damped by the fluid viscosity (Fig. 5.3b). Near the bottom, the shear stress imposed by the water motion to the solid bottom is transmitted almost entirely by the molecular viscosity.

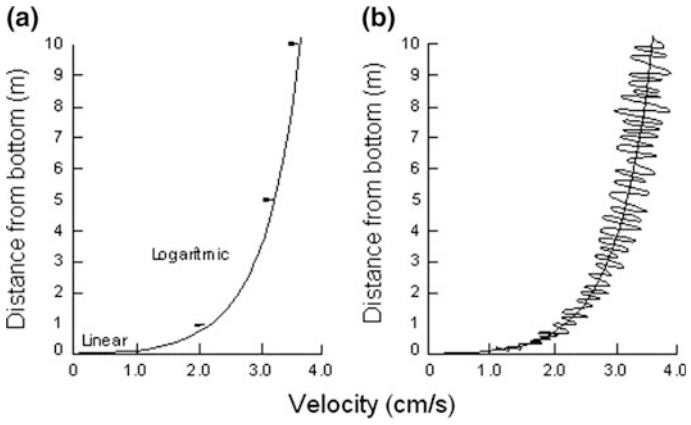

Fig. 5.3 **a** Velocity profile over a smooth bottom surface characterized by the linear viscous sub-layer near the bottom and the upper logarithmic layer. **b** Vertical profile showing the fluctuations and the turbulent motions decrease and turbulent motions in the sub-layer near the bottom (adapted from Chriss and Caldwell 1984)

Figure 5.3a shows a theoretical velocity profile composed of two layers: (i) the logarithmic layer, where the process of vertical diffusion is controlled primarily by small scale motions (Reynolds stress), characteristic of stable stratified estuarine water; and (ii) the viscous sub-layer close to the bottom. To describe these layers, two equations are necessary Chriss and Caldwell (1984); the shear stress (τ) between adjacent fluid layers moving with different velocities is given by:

$$\tau = \rho \nu_c \frac{du}{dz}, \tag{5.9}$$

where ν_c, $[\nu_c] = [L^2T^{-1}]$, is the kinematic coefficient of molecular viscosity, related to the dynamic coefficient calculates by the product $\rho\nu_c$, $[\rho\nu_c] = [ML^{-1}T^{-1}]$, is the dynamic viscosity coefficient.

As the density and the shear stress may be approximated by constant values in this boundary layer, it follows that the ratio $(\tau/\rho)^{1/2}$ is also constant. As this quantity has dimension of velocity $[LT^{-1}]$, it is conventionally defined as the *friction velocity* (u_*), and $(\tau/\rho)^{1/2} = u_*$, or $\tau = \rho(u_*)^2$, which was introduced to represent the shear strength. With the origin of the Oz axis on the bottom and positively oriented upwards, integrating Eq. (5.9), with the adherence principle as the bottom boundary condition, $u|_{z=0} = u(0) = 0$, up to a generic vertical position (z), the vertical velocity profile as a function of the friction velocity (u^*) is:

$$u(z) = \frac{(u_*)^2}{\nu_c} z. \tag{5.10}$$

This equation shows that the horizontal velocity component varies linearly with distance from the bottom (Fig. 5.3a). The viscous sub-layer was always present in the field experiments of Chriss and Caldwell (1984), off the Oregon coast (Oregon, USA) using a fine resolution velocity profiler, and it may be scaled roughly with the ratio (ν_c/u_*) which has dimension of length $[\nu_c/u_*] = [L]$.

Above the viscous sub-layer, the vertical mixing brought about by the turbulence, associated with the bottom friction or shear flows at mid-depth, is of interest itself in the dispersion of a pollutant discharge at a given depth (Bowden 1978). The deflecting influence of the Coriolis acceleration in this layer is not dominant, and may be disregarded. Experiments indicate that in this layer, the horizontal velocity increases in proportion to the logarithm of the distance over the bottom (z). This logarithmic layer, above the viscous sub-layer near the bottom (Fig. 5.3b) is simulated in steady-state conditions, neutral stability and moderate bottom roughness by the following equation (Sverdrup et al. 1942):

$$u(z) = \frac{1}{\kappa}\sqrt{\frac{\tau}{\rho}} \ln\left(\frac{z}{z_o}\right) = \frac{u_*}{\kappa} \ln\left(\frac{z}{z_o}\right), \tag{5.11}$$

assuming $u = 0$ at $z = z_o$. In this equation, $\kappa = 0.40$ (or $\kappa = 0.41$) is a non-dimensional constant of v*on Kármán*, z_o is the depth above the bottom or sea

floor where the velocity is zero (named *roughness dynamic length* or *roughness length*), and is related to the average height of the roughness elements on the bottom (Sverdrup et al. 1942), and u_* (friction velocity) scale the turbulence of velocity. This profile is named the logarithm profile *Kármán-Prandt* and is used to simulate velocity profiles of one-dimensional motions in the continental shelf and estuaries. From this equation we can verify that the velocity profile u(z) and the vertical velocity shear (du/dz) vary linearly with the natural (or neperian) logarithm of the distance z ($\ln(z/z_o)$ down to the bottom, and with the inverse of this distance (1/z), respectively. In both cases, the angular coefficients of the correlations are equal to (u_*/κ); however, the intersection of the straight line with the ordinate axis is equal to the roughness length (z_o) in the first case (Fig. 5.4a), and in the second case it is independent of this length (Fig. 5.4b).

Equations (5.10) and (5.11) assume that the bottom is a plane surface with little roughness. However, in estuaries the bottom is not perfectly plane, and irregularities or roughness elements (tunnels, holes, ripples, sand and gravel) due to erosion, sedimentation, and transport, and benthonic communities generate turbulent shear motions in the bottom viscous sub-layer. If this turbulence is not dissipated by viscosity, the motion regime becomes turbulent and the sub-layer disappears. Despite the erosion of this viscous sub-layer the vertical velocity profile may be approximated by a logarithmic profile which is only related to the vertical exchange of the turbulent momentum. The influence of turbulent motion on the estuary bottom is very important to the sediment dynamics and in solving practical problems related to harbor navigation.

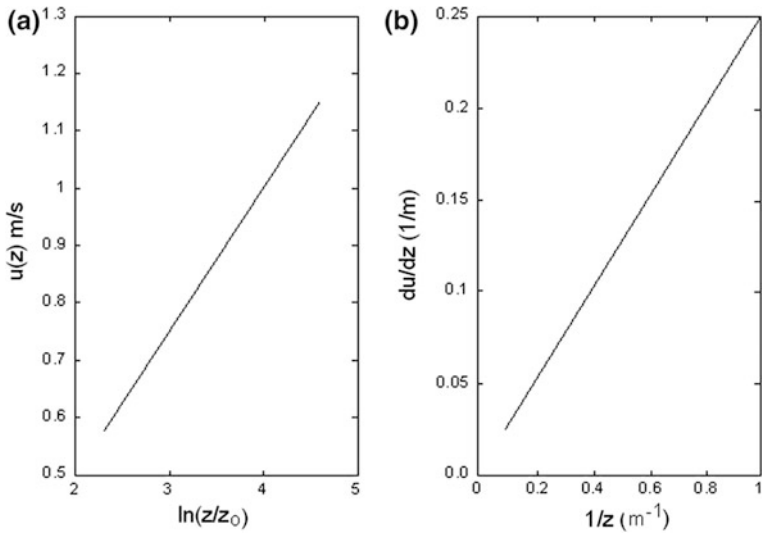

Fig. 5.4 **a** Linear correlations of the logarithmic profile of von Kárman-Prandt, with the ordinate axis representing u = u(z) and **b** du/dz = (1/z), respectively, calculated with $u_* = 0.1$ m s^{-1} and $z_o = 0.1$ m

The rough dynamic length (z_o) is higher in a turbulent flow regime than in the laminar flow regime, and its value has been used to estimate dimensions of irregularities at the bottom. There are several empirical formulations to estimate the z_o value as a function of geometric dimensions, for example, the obstacles mean height and the bottom sand wave slope.

The characteristics of the friction at the bottom (τ_o) in channels forced by the tide were examined by several investigators aiming to relate this shear to a non-dimensional drag coefficient (C_{100}), usually calculated with velocity measurements one meter (100 cm) above the bottom (u_{100}). By analogy with the theoretical result $\tau = \rho(u_*)^2$, obtained for the viscous sub-layer, experimentation indicates that a good quadratic approximation to the coefficient for τ_o is: $\tau_o = \rho C_{100} u_2^{100}$; then, with the assumption that $\tau_o \approx \tau$, it follows that $u_* = (C_{100})^{0.5} u_{100}$. Combining this result with Eq. (5.11), and taking into account that $z = 100$ cm, it follows that $C_{100} = [\kappa/\ln(100/z_o)]^2$. This expression for the coefficient C_{100} depends on z_o, which may be obtained with knowledge of the longitudinal component of the vertical velocity profile plotted as a function of $\ln(z/z_o)$ (Fig. 5.4a). There are also published tables where this quantity is related to the type of the bottom characteristics (Soulsby 1983; Dyer 1986).

Typical z_o values and drag coefficients C_{100} for different bottom types (from mud to gravel), using data drawn from several sources (Lesht 1979 and Heathershaw 1981; quoted in Soulsby 1983), are listed in the Soulsby table according to their observations numbers. The results indicate that the mean z_o and C_{100} values varied from 5.0×10^{-3} to 0.6 cm, and from 1.6×10^{-3} to 6.1×10^{-3}, respectively.

The relationship of C_{100} with z_o was also used by Sternberg (1968) in studies related to friction factors in six tidal channels in the north-west of the USA (Puget Sound and the Strait of Juan de Fuca) divided in two regions (transitional and rough). Among his conclusions, it was identified that the C_{100} value was not very sensitive to the bed characteristics, although the roughness elements of bed types varied from rocks and gravel with maximum heights from 2 to 10 cm, and the mean C_{100} values varied by less than a factor of 2 (2.3×10^{-3}–4.0×10^{-3}). The mean C_{100} value for fully turbulent flow, $C_{100} = 3.1 \times 10^{-3}$, is in agreement with the ranges found in the Soulsby (op. cit) table.

Another interesting conclusion of Sternberg's article is that the transition between fully rough and transitional flow appears to be related to the bottom configuration, and for simple topographically beds the flow becomes fully rough at lower Reynolds numbers (less than 1.5×10^5) than those with complex seabed topographical seabed, for which rough flow conditions occurred at Reynolds number (R_e) greater than 3.6×10^5.

The *profile method* uses Eq. (5.11) with experimental data of vertical velocity profiles to calculate the friction velocity (u_*) and the rough length (z_o) and uses the relation $\tau = \rho u_*^2$ to estimate the shear stress on the bottom. This method is the most commonly used to estimate the shear stress of geophysical fluids in shallow waters (channels, estuaries and continental shelf).

This method has been applied to several oceanographic conditions and coastal environments. In estuaries, the pioneering experiments were performed after the

1920 decade, thanks to the works of Merz (1921) and Mossby (1947). The experimental data used by these investigators (vertical velocity profiles) were sampled in the Dardanelles fjord (Denmark) and in the Avaerströmmem fjord (Bergen, Norway), respectively. The historical data of A. Merz published in the Defant (1961) book and reproduced in Fig. (5.5a) is an example of the method used to determine the analytical expression of the logarithmic velocity profile. The first member of the left-hand side of Eq. (5.11) is known at discrete points in the water column; however, in the second term, there are two unknowns, u_* and z_o. An alternative way to eliminate one of these unknowns is to calculate the derivative of this equation in relation to z, resulting in the following expression u_* being the only unknown:

$$\frac{du}{dz} = \frac{u_*}{\kappa}\frac{1}{z}. \tag{5.12}$$

This equation shows that the vertical velocity shear (du/dz) is inversely proportional to the distance from the bottom (z). As the first member of this equation may be determined by finite differences ($du/dz \approx \Delta u/\Delta z$) with experimental data (Fig. 5.5a), the angular coefficient of the linear correlation of this quantity with 1/z is equal to the ratio u_*/κ (Fig. 5.5b) This procedure results in the following value for this ratio: 2.5×10^{-2} m s^{-1}. As the constant k = 0.40, it follows that the value for $u_* = 1.10 \times 10^{-2}$ m s^{-1}.

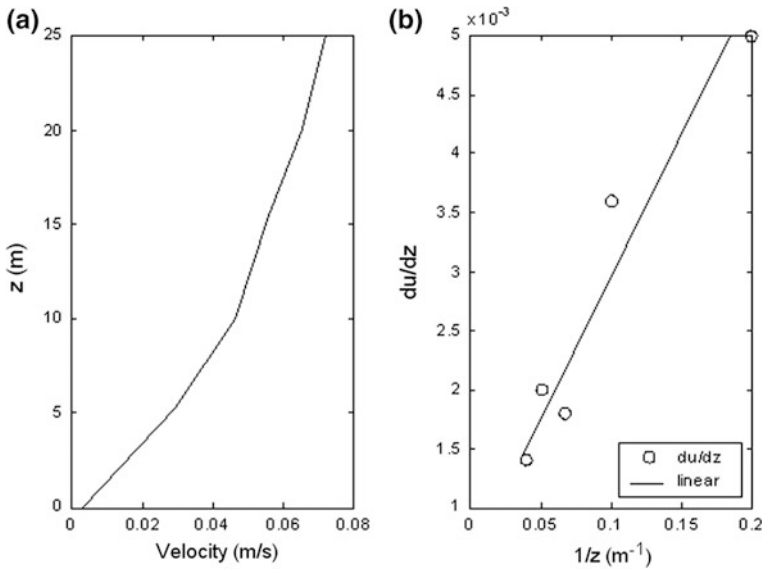

Fig. 5.5 **a** Vertical velocity profile in the south entrance of the Dardanelles estuary (Denmark), with data sampling by Merz (1921). **b** Correlation of the vertical velocity shear ($\Delta u/\Delta z$) as a function of (1/z) (*open dots*) and the linear adjustment

With the calculated value of u_*, the *rough dynamic length*, z_o, of the logarithmic profile (Eq. 5.11) may be obtained with successive adjustments, up to the best linear fit in comparison with the experimental data. Several values were tested, with the best fit found to be $z_o = 1.5$ m as shown in Fig. 5.6. Then, with this method, the experimental data is analytically formulated by the following logarithmic profile:

$$u(z) = 2.5 \times 10^{-2} \ln\left(\frac{z}{1.5}\right), \tag{5.13}$$

with the ordinate z and u(z) in SI units (m and m s^{-1}), respectively. As the shear stress ($\tau = \rho u_*^2$) is proportional to the square of the friction velocity, the value of this physical quantity was estimated to be ≈0 0.11 N m^{-2}, with the assumption $\rho = 1.02 \times 10^3$ kg m^{-3}.

Theoretical simulation of the logarithmic profile is not always possible from the surface down to the bottom, and the water layer from the bottom up to the best fit is named *height of the logarithmic layer*, h_L, (Lueck and Lu 1997). In the exemplified adjustment of the logarithmic profile (Fig. 5.6) this height reached 15 m.

The mean vertical velocity profile used in this example is unidirectional, which is characteristic of a well-mixed estuary. However, due to the gravitational circulation forcing, the time variability of the velocity during a tidal cycle may be unsteady, and so the vertical velocity profiles are as shown in Fig. 2.9 (Chap. 2). In partially mixed estuaries, the vertical velocity profiles indicate the occurrence of seaward and landward motion, and it will be impossible to simulate their logarithmic velocity profiles.

Vertical velocity profiles in estuaries are often difficult to be sample over several tidal periods, particularly in harbors which may experience intense maritime traffic, or due to the weather conditions. However, investigations in estuaries increased substantially in the decades following on the historical experiment in fjords, as described above, improving the knowledge of these transitional water bodies. Further results based on logarithmic profile adjustments are presented in Dyer (1986).

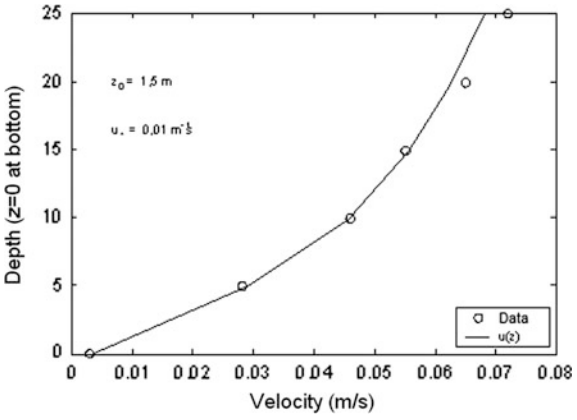

Fig. 5.6 Adjustment of the logarithmic profile to experimental data (o) measured in the Dardanelles estuary (Denmark), presented in the classical article of Merz, in 1921, in which $h_L = 15$ m

To describe results of the application of the profile method, based on detailed time series of bottom-mounted acoustic Doppler profiles (ADP), this topic is complemented with results from the experiments of Lueck and Lu (1997). In this experiment 20-min time averaged velocity profiles at 30 m depth were made in the Cordova channel near Vancouver Island (Canada). The time series of current measurement where made during 4.5 days, with the objective to study the local variability in the bottom-boundary layer at 3.6 m and the current profile variability above this depth. In this investigation, the friction velocity (u_*) based on the logarithmic profiles, the time variability of the logarithmic height (h_L) and the rough dynamic length (z_o) were calculated.

The vertical velocity profiles measured during a time interval of 1.5 days are one-directional during the ebb (>0) and flood (<0) tides, and their logarithmic adjustments are presented in Fig. 5.7. A well-defined logarithmic layer is observed during the events of intense tidal currents, where height (h_L) is in the top half of the water column; however, logarithmic adjustments were not possible during the time intervals of low current intensity.

An alternative method to calculate the shear stress is possible with the introduction of a non-dimensional drag coefficient, C_D. This coefficient is often used in analytical and numerical models to parameterize the bottom frictional shear as a function of a velocity of reference (U_r) according to the following expression:

$$\frac{\tau}{\rho} = C_D U_r^2, \tag{5.14}$$

or, taking into account that $\tau/\rho = u_*^2$,

$$C_D = \left(\frac{u_*}{U_r}\right)^2. \tag{5.15}$$

The friction velocity (u_*) may be determined from the logarithmic profile and can be used to calculate C_D (Eq. 5.15). As the u^* velocity is known, it is adequate to select the reference velocity in the viscous sub-layer from the velocity profile. The

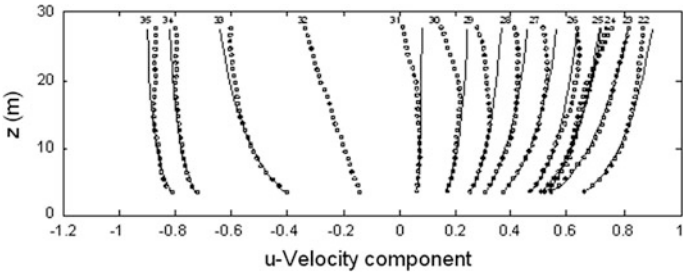

Fig. 5.7 Vertical velocity profiles of the longitudinal component (o) in the Cordoba channel (Vancouver, Canada). The analytical simulations of the logarithmic layer are indicated by the *continuous lines* (according to Lueck and Lu 1997)

ebb and flood velocity profiles (Fig. 5.7) were used to calculate this coefficient during a tidal cycle, using as reference velocity (U_r) the following velocity values: the mean velocity in the water column (u_m), the velocities at the heights of 1.0 m (u_{100}) and 3.6 m (u_{360}) above the bottom. According to the results, the lower values of this coefficient were observed during the ebb tide currents ($u > 0$): $3.5 \times 10^{-3} < C_D < 8.8 \times 10^{-3}$, with the extreme values obtained for the u_m and u_{100} as reference velocities. During the flood tide currents ($u < 0$), the variation interval of this coefficient was higher: 4.0×10^{-3}—2.5×10^{-3}.

As indicated above, simulation of logarithmic velocity profiles in tidal estuaries is very important to provide clues on the friction shear at the bottom. However, it may only be applied for estuaries with predominating longitudinal velocity profiles (seaward and landward), which are characteristic of well-mixed estuaries. Analytical simulations of well-mixed, partially mixed and salt wedge estuaries, in steady-state conditions will be studied later using the hydrodynamic equations of motion. The vertical profiles of scalar properties, such as temperature, salinity and density usually have no simple analytical and numerical simulations, and for these properties numeric values at non-sampled depths may be determined at selected depths by numeric (*cubic splines*) or graphical methods.

5.3 Temporal and Spatial Averages

The superposition of motions generated by tide, river discharge, baroclinic gradient pressure force and wind, create difficulties in the experimental data treatment and processing, and demonstrates the convenience of using mean values in time and space to calculate an estuary's nearly steady-state condition. To better understand the estuarine processes, we must be able to separate those forcing influences (Dyer 1997).

Measurements of hydrographic properties and current velocity are sampled at selected positions (stations) and discrete time intervals, or continuous in time and space. The selection of a suitable sampling duration to determine the time-averaged estuarine condition is as critical as the spatial sampling. Then, to obtain instantaneous or mean values of these properties and the steady-state circulation, it is necessary to adequately reduce these measurements taking into account the following criteria and results to be accomplished:

(i) Make the data analysis easier;
(ii) Obtain average properties for estuary classification;
(iii) Validate theoretical results of analytical and numerical models;
(iv) Determine the advective and diffusive components of salt flux and transport, and the net transport of natural substances and pollutants.

In the determination of mean velocity profiles and other properties (hydrographic, chemical, biological, and suspended sediment), it is necessary to take into

account that the local depth is dependent on the position and time, which may vary greatly due to the tidal oscillation, η(x, y, t), during the measuring period. This is because the local depth at any given time is h(x, y, t) = H_0(x, y) + η(x, y, t), with H_0 and η representing mean water level and the tidal oscillation, respectively. The non-dimensional number defined by the ratio of the tidal height (H_o) to the local depth h(x, y, t) varies in the interval $0 < |H_o|/H_0| \leq 1$. If the tidal height (H_o) is greater than 30% of the $\text{local}_{\text{depth}}$ (H_0),

$$\frac{|H_o|}{|H_0|} > 0.3, \tag{5.16}$$

this ratio is relatively great in comparison to the water depth, and the time variation of the sampling depths must be minimized in the determination of the mean vertical profiles of the properties, as prescribed in the articles of McAlister et al. (1959) and Kjerfve (1975).

Thus, the periodic fluctuations of the water column layer due to the tidal oscillation cause variations in the sampling depths along the water column. If these depth variations are not taken into account when determining the mean values in space and time, undesirable errors may occur when the inequality expressed in (5.16) is reached. This correction may be accomplished by determining data values at equally spaced distances between the surface and bottom, with the non-dimensional depth Z(t), which depends on the origin (z = 0) and the orientation of vertical ordinate Oz:

(i) If this origin is at the bottom (positively oriented towards the surface level), h(t) is the water layer depth and z is the ordinate of the sampling depths, Z(t) is defined as,

$$Z(x, y, t) = \frac{z - h(t)}{h(x, y, t)}, \tag{5.17a}$$

and varies from zero (Z = 0) for one observation at the surface, z = h(t), to (Z = −1), for the observation at the bottom, z = 0.

(ii) If the origin of the vertical ordinate is at the surface and positively oriented against the gravity acceleration, the dimensionless depth is defined by,

$$Z(x, y, t) = \frac{z}{|h(x, y, t)|}. \tag{5.17b}$$

Thus, the non-dimensional depth, Z(x, y, t), and varies from 0 (surface) up to Z = ±1 (bottom), and the signal depends on the Oz axis orientation. In numerical modeling Z(x, y, t) is called the *Sigma* coordinate.

As one of the objectives of estuarine research is to describe the spatial and local distribution of properties, a common survey goal is to obtain the circulation of a particular estuary and the net movement, flux and transport of dissolved or suspended constituent. In both cases it is necessary to compute time-averages of tidal cycles over at least one complete tidal cycle. Due to the expansion and contraction of the water column height in the flood and ebb tide, this is better accomplished with data processing in terms of the non-dimensional depth, Z(x, y, t). This procedure is illustrated in the temperature and salinity profiles measured in an estuarine channel that is partially mixed estuary (Fig. 5.8). The comparative analysis of these properties as a function of the dimensional (z) and non-dimensional (Z = z/7.5) depths, shows the conservation of the profile configurations from the surface down to the bottom.

With the changes from dimensional (z) to the non-dimensional depth (Z), mean depths values of properties may be calculated even in the most unfavorable conditions (Eq. 5.16). After, considering the non-dimensional depth form, each measured property may be interpolated at each non-dimensional depths (Z = 0; Z = 0.1; … Z = 0.9 and Z = 1.0), as illustrated in Fig. 5.9.

Discrete measurements should be made at a constant time interval (Δt), over at least one complete tidal cycle. However, if at all possible, sampling should be continued for the sampling duration indicated by Eq. (4.1, Chap. 4) as net values may vary drastically from one tidal cycle to the other. It is suggested that the initial time measurement (t_0) should begin at slack water (close to the low or high tide)

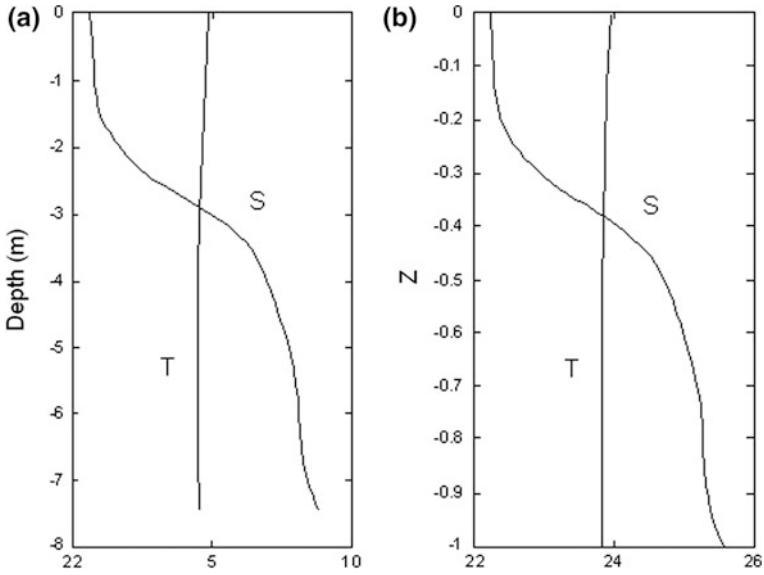

Fig. 5.8 Vertical salinity, S = S(z) and S = S(Z), and temperature T = T(z) and T = T(Z) profiles as functions of dimensional (**a**) and non-dimensional depths (**b**). Oz is positively oriented upward

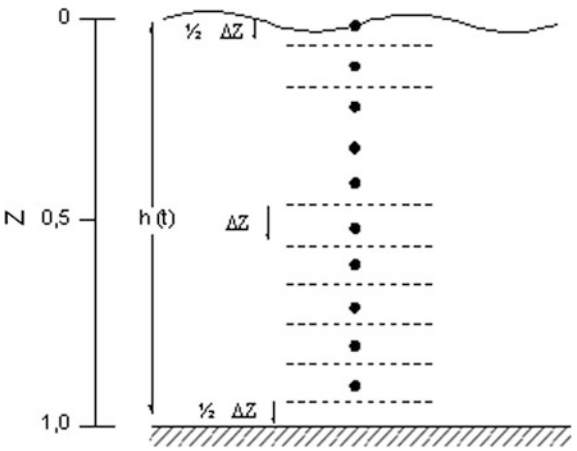

Fig. 5.9 Water column with discrete equidistant non-dimensional depth intervals ΔZ and (1/2)ΔZ of the non-dimensional depth (Z)

and at time intervals, Δt, of one or half hour (1.0 or 0.5 h) to minimize possible averaging errors. In the case of continuous sampling, the time series must be interpolated for analytical analysis at the Δt interval just specified. Usually, for a particular tidal cycle period (T_P), we have $T_P = n\Delta t$ (and $n = T_P/\Delta t$), where (n + 1) is the number of required profiles to compute the net profile for a given tidal cycle. Typically, in semi-diurnal or mixed tide regimes, if *n* is selected to be 12.4 h, the sampling rate equals 1.035 h or one *lunar hour* (Bowden 1963; Kjerfve 1975). In such cases, it is necessary to plot curves of each variable at all Z-depths as functions of time and then divide each time series into *n* equal increments. The interpolated values for each Z, at n + 1 times would then be used in computing time averages.

If the net value of one measured property, P, at a given non-dimensional depth, Z (Z = 0.0; 0.1; 0.2;…, 1.0) is expressed as a function of time P(Z, t), its time mean value during a tidal period (T_P) and at each depth is indicated generically by Z_j (j = 0, 1, 2, …, 10), and are calculated by:

$$\langle P(Z_j) \rangle = \frac{1}{T_P} \int_0^{T_P} P(Z_j, t)dt, \tag{5.18}$$

where the symbol ⟨⟩ indicates the time mean value of the property. Taking into account that the values $P(Z_j, t)$ were obtained in *n* discrete interpolations at constant time intervals, Δt ($T_P = n\Delta t$), the integral of Eq. (5.18) may be easily calculated for each depth (Z_j) by the following sum:

$$\langle P(Z_j) \rangle = \frac{1}{n} \left[\frac{P(Z_j, t_0)}{2} + \sum_k P(Z_j, t_k) + \frac{P(Z_j, t_n)}{2} \right], \tag{5.19}$$

where k = 1, 2, …, n − 1, and t_1 and t_n are the first and last time measurements and $(t_n - t_0) = T_P$ is the tidal period. In this equation, the property values at the initial and final time (t_0 and t_n) are multiplied by the factor ½, because it is assumed that each of these values are representative for only (½ Δt), as shown in Fig. 5.10. It should be noted that the time mean value at a generic depth, $\langle P(Z_j) \rangle$, may be almost independent of time (nearly steady-state).

Equation (5.19) applied for j = 0, 1, …, 10, may be used to calculate the mean vertical profiles of any scalar property: velocity component, temperature, salinity, and concentrations of nutrients and suspended sediments. When applied to the salinity, the time mean values simulate nearly steady-state conditions and the surface (S_s) and bottom (S_f) values may be used to determine the stratification parameter, $\delta S / \langle \overline{S} \rangle = (S_f - S_s) / \langle \overline{S} \rangle$ of the Stratification-circulation Diagram. Measurements of properties along the transverse section of the estuarine channel may also be processed in the same way to calculate mean property profiles.

As the velocity is a vector, the method used to calculate its mean value during tidal cycles is applied to the longitudinal (u) and transversal (v) components, which may be obtained with the procedure described in this paragraph. For instance, to find the longitudinal component, the temporal mean value is determined for each non-dimensional depth Z_j with an equation similar to (5.19):

$$\langle u(Z_j) \rangle = \frac{1}{n} \left[\frac{u(Z_j, t_0)}{2} + \sum_k u(Z_j, t_k) + \frac{u(Z_j, t_n)}{2} \right], \tag{5.20}$$

where k = 1, 2, …., n − 1.The mean u-velocity component on the surface corresponds to the u_s value, which simulates a nearly steady-state value and is used to calculate the circulation parameter (u_s/u_f) of the Stratification-circulation Diagram.

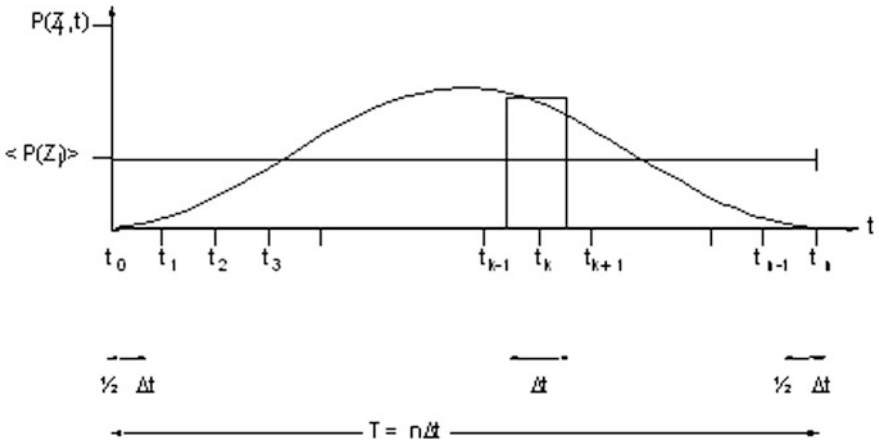

Fig. 5.10 Schematic sequence of time measurements. At the initial (t_0) and final (t_n) times the measured property is assumed to be representative for ½ (Δt) time interval

To calculate the time-mean value of the transversal velocity component (v) this value must be used in Eq. (5.20) as a substitute for the u component.

Once calculated, the time-mean velocity u and v components for the velocity vector at each depth along the water column may be calculated by the vectorial composition:

$$\left\langle \vec{v}(Z_j) \right\rangle = \left\langle u(Z_j) \right\rangle \vec{i} + \left\langle v(Z_j) \right\rangle \vec{j}, \tag{5.21}$$

where $\vec{i}$ and $\vec{j}$ are the unity vectors of the coordinate system used. This computation of time mean velocity components during tidal cycles is very important because: (i) it indicates the net flow which is a characteristic of import and export of property concentrations, and; (ii) it may be used to validate analytical and numerical models (for a bi-dimensional numerical model this procedure has been used by Blumberg 1975).

Let's now consider a property profile P = P(z, t) or P = P(Z, t) in a determined time. The mean value ($\overline{p}(t)$) in the water column ($0 \leq z \leq h$ or $0 \leq Z \leq 1$) is given by:

$$\overline{P}(t) = \frac{1}{h} \int_0^h P(z, t) dz = \int_0^1 P(Z, t) dZ, \tag{5.22}$$

where the over bar indicates a spatial mean, in this case the depth z and Z, and taking into account that, by definition, $dz = |h| dZ$.

As this integral (Eq. 5.22) must be calculated from known values at discrete points along the water column, for example, spaced $0.1\Delta Z$, its mean value is calculated by an equation similar to (5.19),

$$\overline{P}(t) = \frac{1}{10} \left[\frac{P(0, t)}{2} + \sum_j (P(Z_j, t) + \frac{P(-1, t)}{2} \right], \tag{5.23}$$

where j = 1, 2, …, 9. When the property P(Z, t) is substitute by the velocity components (u, v) and the no-split condition of the adherence principle at the bottom adopted for the bottom friction (null velocity), the extrapolation down to the bottom of the last parcel in this equation is null, because $u(-1, t) = v(-1, t) = 0$.

5.4 Reduction and Analysis of Temporal Data Series

Time series of properties' measurements of short or long duration may have their analysis performed in the time domain and in the frequency domain with spectral techniques. For example, in the first case the analysis of the current may be made at selected depths in the form of vector plotted sequentially in time in the graphic

known as a *current rose* and as a *progressive vectorial diagram*, usually applied for experiments of only a few tidal cycles. The theory evolved in the spectral analysis is not presented in this text, and may be found in the following books: Bendat and Piersol 1966; Rayner 1971; Jenkins and Watts 1968; Moretin 1999. Its importance will be exemplified with hourly time series of tidal height, salinity and temperature.

To give an example, the time series analysis was made for a half-hour current measurements (intensity and direction) at an anchor station during one spring tidal cycle in the Caravelas river estuary (Bahia, Brazil). The station is in the position where the channel orientation is approximately in the E-W direction (Chap. 12, Fig. 12.7). The current roses (Fig. 5.11) show the velocity vectors plotted during the semi-diurnal tidal period at two selected depths Z = 0 and Z = −0.9, at surface (left) and near the bottom (right). The analysis of these results indicate the gradual decrease of the intensity with depth, and changes in the current directions during the tidal cycle; from the surface down to mid-depths the current is mainly towards east (90°), indicating an ebb motion with maximum speed of ≈1.3 m s^{-1} (Fig. 5.11-left). At the middle of the tidal cycle the tidal current direction changed towards the west (270°), indicating the tidal flood with maximum intensity of ≈0.9 m s^{-1}. Close to the bottom (Z = −0.9) the maximum current intensity is ≈0.6 m s^{-1} seaward, and due to the baroclinic gradient pressure force, the direction of the current changes towards west (270°), indicating the motion forced by the tide flood with slightly higher intensity (≈0.7 m s^{-1}) than in the surface (Fig. 5.11-right).

The current roses also indicate that the transverse circulation is very weak, which also is shown in the comparison of the time variation of the u- and v- velocity components (Fig. 5.12), which clearly indicates that the main advective influence is in the estuary longitudinal direction.

As should be expected, the progressive vector diagram shown in Fig. 5.13, plotted with the u-and v-velocity components of the previously data used in figure

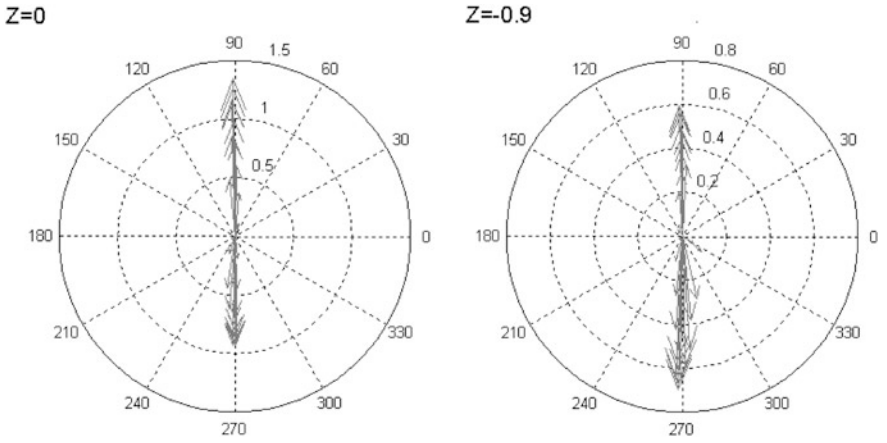

Fig. 5.11 Current roses from half-hourly measurements at the surface (*left*) and near the bottom (*right*), in the Caravelas river estuary (Bahia, Brazil) during spring tide

(Fig. 5.12), indicates the predominance of the longitudinal motion and almost negligible transverse motion. At the surface the particle excursion during the flood and ebb are approximately 22 and 17 km, respectively, and near the bottom the particle excursion is shorter (≈9 km) in the ebb than in the flood (≈13 km).

The time variation of the scalar properties temperature, salinity and density (Sigma-t) at the surface (Z = 0) during the spring tidal cycle, associated with the velocity (Fig. 5.11), are presented in Fig. 5.14. The small temperature variation ($\Delta T \approx 0.8$ °C) indicated that the salinity is the main property responsible for the density variation, as also shown in the Sigma-t time variation. Near the bottom the hydrographic properties indicates small variations in comparison to that observed in the surface.

To give an example of time series spectral analysis in practice, three simultaneous records measured during 20.8 days in the estuarine channel of the Cananéia sea (Fig. 1.5, Chap. 2) located in the southern São Paulo State (Brazil) have been analysed. The tidal height time series was registered in a recording buoy tidal gauge and the tidal height values (cm) were digitalized with half hour time intervals ($\Delta t = ½$ h). Simultaneous temperature (°C) and salinity (‰) measurements were recorded at the same time interval in digital format by the equipment positioned 6.0 above the bottom. These Eulerian measurements were sampled in 10 m mean water depth, and the time variability of these properties (In Julian days) is presented in Fig. 5.15.

The tidal height oscillations show semidiurnal variations superimposed to fortnightly tidal modulations, with amplitudes higher in the spring tide than in the neap tide. The visual time series analysis of salinity and temperature records follow the general trend of the tidal oscillations, showing a quick response to the advection of salt and heat transport generated by the tidal currents. During the spring tidal oscillations, the amplitudes of these properties vary more than during the neap tide, and it is possible to visualize low frequency variations within periods of several days. However, these temporal variations do not show details of the correlations between tidal, salinity and temperature oscillations related to its time, periodicity and phase variations.

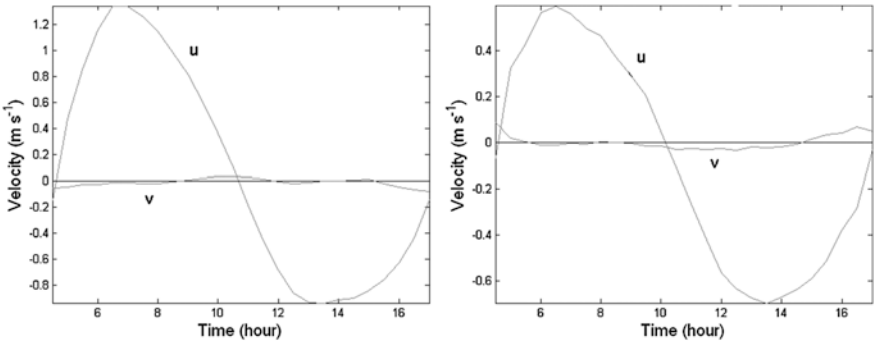

Fig. 5.12 Time variation of the u- and v-velocity components at the surface (*left*) and near the bottom (*right*) measured in the Caravelas river estuary (Bahia, Brazil) during spring tide

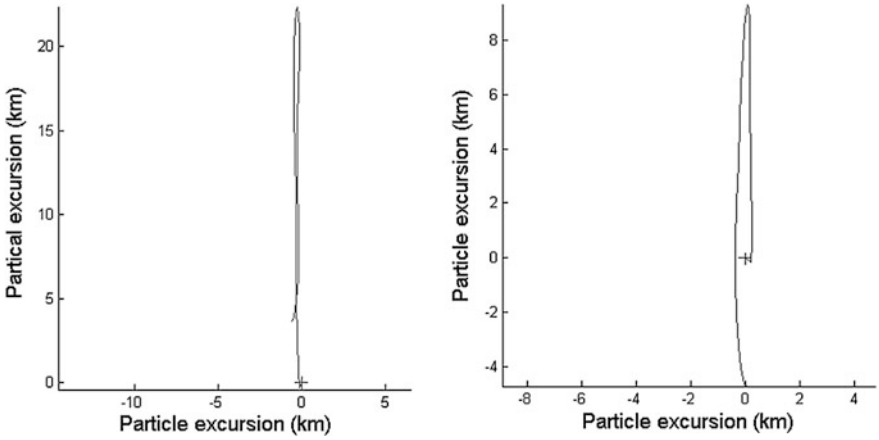

Fig. 5.13 Progressive vector diagram at the surface (*left*) and near the bottom (*right*), based in current measurements measured in the Caravelas river estuary (Bahia, Brazil) during spring tide. The initial position of the diagram is indicated by the plus (+) symbol

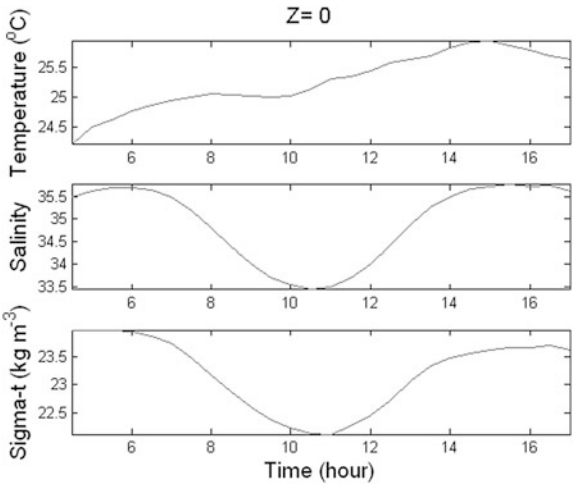

Fig. 5.14 Time variation of the hydrographic properties at the surface (Z = 0) measured in the Caravelas river estuary during the spring tidal cycle (Bahia, Brazil)

The spectral analysis determines the variance in frequency bands. The variance is a statistical quantity which describes the dynamic component of the time series, numerically calculated by the quadratic mean value around its mean value. In the *variance spectra*, it is possible to do the analysis of the dynamical component intensity of these properties as function of frequency. The frequency band for which the variance may be estimated has two limiting factors: the time series length, $T = n\Delta t$, and the sampling interval, Δt. For the records of Fig. 5.15, these values are equal to 20.8 and 0.5 h, respectively.

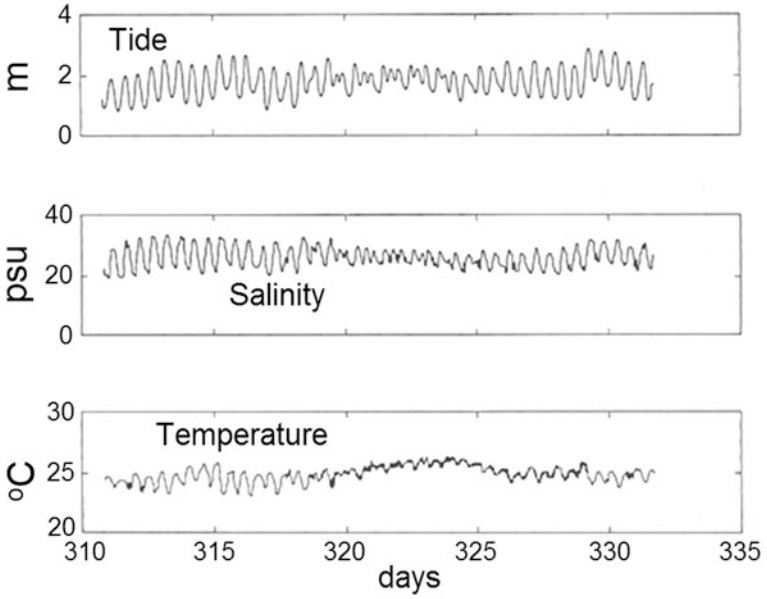

Fig. 5.15 Time series of tidal height, salinity (psu) and temperature (°C) in the microtidal Cananéia estuarine channel (time scale in Julian days)

The time series length determines the lowest frequency for which the variance may be estimated, which is equal to the inverse of the series time length (1/T), and, in our example, corresponds to the frequency of 0.048 cph. The highest frequency for determining the variance is called the *Nyquist* frequency, which is half of the sampling frequency (f_s). As the sampling interval is 0.5 h, it follows that $f_a = 2$ cph, and the *Nyquist* frequency is equal to ($\frac{1}{2}$ $f_a = 1.0$ cph); the variance calculated for this lower frequency may not be representative because, for this quantity to have statistical meaning, it must be determined taking into account three or four complete tidal cycles. Due to this limiting factor, for the 20.8 day time series under analysis, the longest period that may be adequately resolved is approximately five days (period of 120 h and frequency of 0.008 cph).

The sampling time interval chosen is very critical. If the property presents variability with frequencies higher than the *Nyquist*, the spectra may present a doubtful increase in low frequencies. This change of the variance from high to low is called *aliasing*. Then, the correct use of the sampling time interval (Δt) is of fundamental importance to apply the techniques of the spectral analysis to observational oceanographic data. In estuaries the Δt equal to one or half an hour is usually satisfactory, because the more energetic variance signals are associated with tidal oscillations, with diurnal od semi-diurnal cyclic oscillations (frequencies of 0.04 and 0.08 cph, respectively).

The variance determinations are calculated at regular frequency intervals between the extreme points of the domain. The number of variance estimates in this

interval is fixed by the total number of points in the time series divided by the degrees of freedom. The choice of variance requires a compromise between the following conflicts of interest: (i) an increase in the degrees of freedom determines narrows confidence intervals, (ii) a decrease in degrees of freedom increases the frequency resolution. The latter compromise is favorable when analyzing long time series. In choosing degrees of freedom, it is necessary to take into account the frequency interval which has the greatest interest to the processes being investigated. For better resolution at lower or higher of frequencies, it is necessary to choose the data processing with low or high degrees of freedom, respectively. Details for obtaining confidence intervals as functions of the degrees of freedom, which are of fundamental importance to the verify the statistical meaning of the variance results, may be found in the book of Bendat and Piersol (1966).

In the tidal variance spectra (Fig. 5.16a), it is possible to understand what processes influence this dynamical component of the sea level oscillations. In this figure, the extreme points (peaks) in the variance, A, B, C, D and E, between the domains of low and high frequency, respectively, were inserted to facilitate the understanding of the analysis of this spectra calculated with 5 degrees of freedom. In these spectra peaks, the variances are statistically confident within the 95% interval. The estimated variances for the frequency band A (0.012 cph—period of 83 h) are too low to be adequately solved. This peak (A), although with little significance, is usually associated with meteorological forcing causing storm surges against the coastline (Csanady 1982). The remaining peaks are oscillations with the following frequencies and periods, respectively: diurnal (B) with 0.04 cph and period of 25.0 h, semidiurnal (C) with 0.08 cph and period of 12.5 h, and the frequencies in the sub-tidal domain (D) and (E), with frequencies of 0.12 and 0.16 cph, and periods of 8.2 and 6.2 h.

The salinity variance spectra (Fig. 5.16b) is very similar to the tidal variance spectra, and conclusively indicates the advection process forced by the barotropic gradient pressure force (tidal forcing) in the salinity redistribution in the Cananéia main channel.

The generation of internal overtides at multiples of the dominant tidal frequency is termed *barotropic tidal asymmetry*, because it distorts the free surface and causes flood or ebb dominant currents, depending on the relative phases of the tides and its overtides (Fisher et al. 1972; Ianniello 1977; Simpson et al. 1990; Jay and Musiak 1996). Factors such as friction and channel morphology generate shallow water over tides such as M_4 and M_6. When these tidal components are added to M_2 tidal current, maximum ebb and flood may be shifted close to high and low water, resulting in a strong tidal current that is distorted from that generated by the semi-diurnal M_2 tidal component.

Another important result is the cross-correlation between the tidal and salinity time series. From this correlation, two spectra results: (a) *covariance* or *normalized coherence*, calculated by the ratio of the product of covariance to the individual square roots, and; (b) the *phase spectra* (Fig. 5.17a, b). The covariance is a non-dimensional quantity, which varies between zero and one, and measures any linear relationship between the individual series, and values equal to zero and one indicate no correlation or a strong linear correlation between the series and

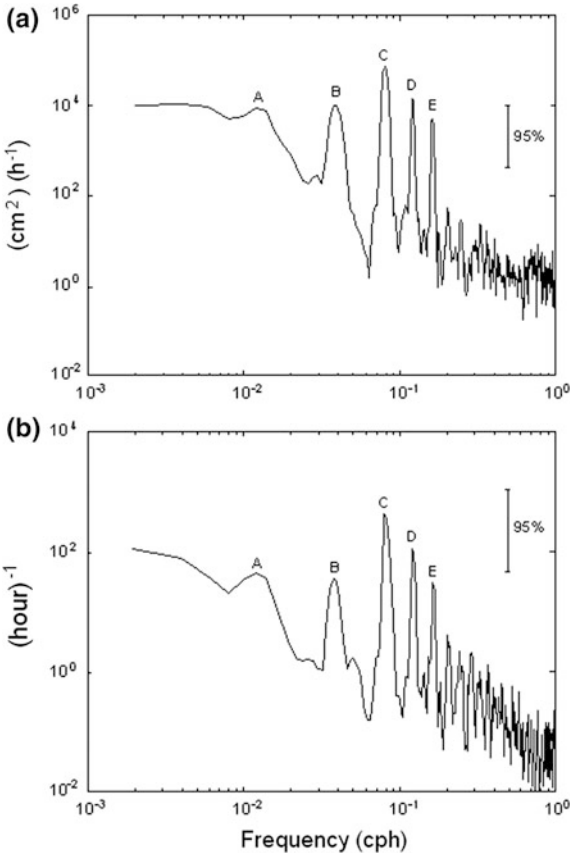

Fig. 5.16 Variance spectra of tidal height oscillations (**a**) and salinity (**b**) as functions of the frequency in cph in the main channel of the Cananéia-Iguape estuarine lagoon (Fig. 1.5, Chap. 1) showing variability of the tidal oscillation and salinity

processes, respectively. This quantity may be identified as a correlation coefficient in the frequency domain.

In the covariance spectra, exemplified by the cross correlation of tidal height versus salinity (Fig. 5.17a), the 95% statistically significant variance with 5 degrees of freedom has a coherence of over 0.9 in the low frequency domain (0.012 cph and period of 83 h) and for diurnal frequencies (0.04 cph and period of 25 h). In the semi and three-diurnal frequencies (periods of 0.08 and 0.12 cph), the coherence is close to 1.0, decreasing just a little near the frequency of 0.16 cph (fourth-diurnal) as shown in Fig. 5.17b. These results indicate that in these frequency bands there are a very strong linear correlation between the tidal height and the salinity.

The final result of the spectral analysis is the phase spectra (Fig. 5.17b), which gives the phase differences between the series. The phase angle (ϕ) may be converted into time intervals when divided by the product of the angular frequency (ω) by $360°/2\pi$, $\Delta t = \phi/(\omega \times 360°/2\pi)$. Then, for example, the diurnal component of the salinity oscillation is in phase with the tide ($\phi \approx 0°$) and the semi-diurnal component is 20° out of phase, or $\Delta t = 0.7$ h in relation to the tide.

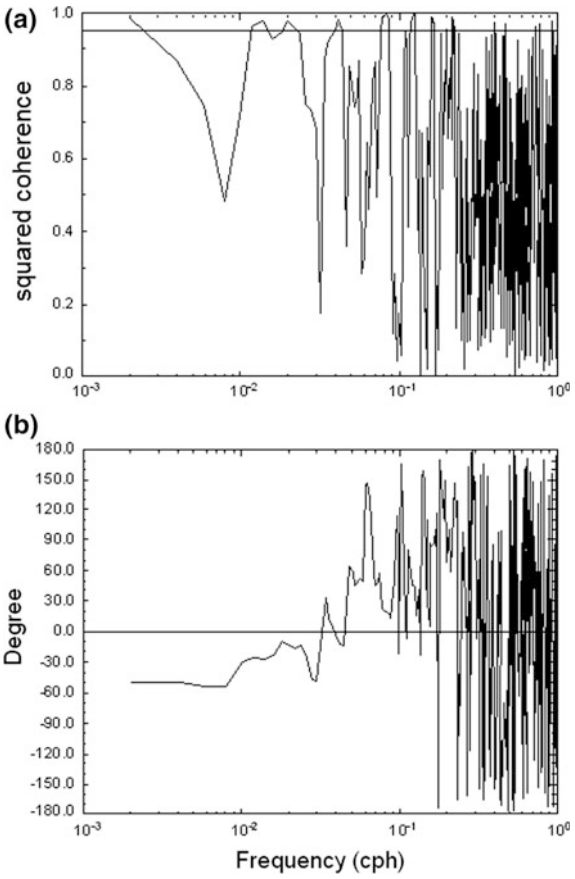

Fig. 5.17 Coherence normalized spectra (**a**) and phase spectra (**b**) of the cross-correlation of tidal heights and the salinity in the main channel of the Cananéia-Iguape estuarine lagoon (Fig. 1.5, Chap. 1)

The spectral analysis is a powerful mathematic tool for quantifying the linearity (or non-linearity) between time series with complex variability. However, the interpretation of its results must be made with caution, because statistically significant coherence values may not necessary imply cause and effect in the occurrence of linear relationships. Small coherence values suggest non-linearity, but there is the possibility of the existence of relationships between the physical forcing processes.

5.5 Isopleths Method and Mean Vertical Profiles

After the reduction and final data processing of hydrographic variables and current velocity components (u, v), graphical representation is necessary to enable interpretation and analysis of the experimental results. When the measurements are made at a fixed station along the water column for a duration of at least one

complete tidal cycle (Eulerian sampling), the isopleths method is convenient for studying the variability of properties under investigation.

In Fig. 5.18, results are presented for the local variability of the u-velocity component and salinity in the Bertioga estuarine channel (Fig. 1.5, Chap. 1), during two semi-diurnal spring tidal cycles (≈25 h), measured at a fixed station at hourly time intervals. The tidal oscillation and the u-velocity time variations are asymmetric (Fig. 5.18-upper), and the highest velocities (≈0.8 m s^{-1}) during the ebb have a phase difference of ≈2.5 h in relation to the HW; however, at the flood the intensities are very low (≈0.2 m s^{-1}).

The temporal salinity variation (Fig. 5.18—lower) indicates that the estuarine channel is highly stratified, and at HW and LW the salinity values are 36.0 and 22.0‰, respectively. The salinity differences between the bottom and the surface are up to 14 and 6‰ at HW and LW, respectively, and nucleus with maximum values (36‰) indicate the Tropical Water mass (TW) intrusion into the estuary. The phase difference between the u-velocity component and the tidal oscillations usually observed in partially-mixed estuaries (Hunt 1964), is mainly due to frictional energy dissipation at the bottom. It is also possible to observe at low tide the

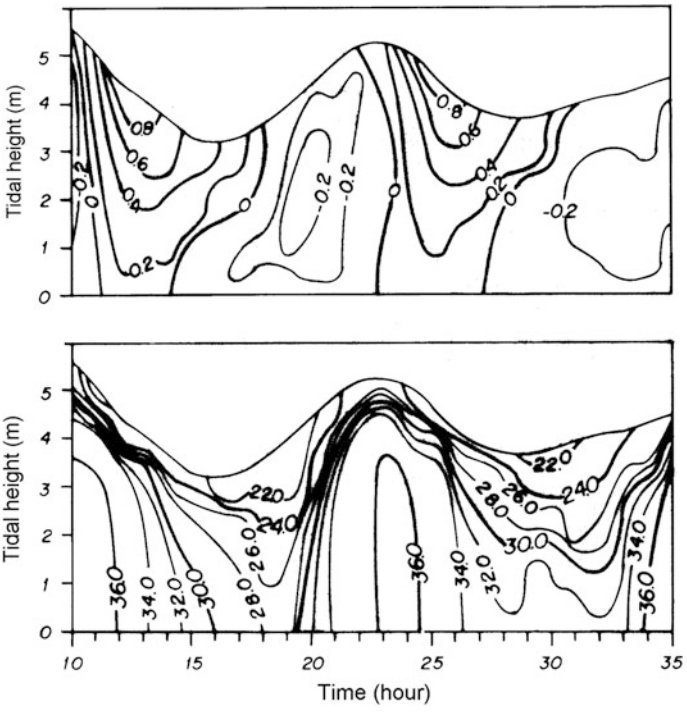

Fig. 5.18 Isopleths of the u-velocity component (m s^{-1}) (*upper*), and salinity (‰) (*lower*) in the Bertioga estuarine channel (São Paulo, SP, Brazil) during spring tide, which are in phase with the slack water (u = 0). Positive and negative velocity values indicates flood and ebb currents, respectively (after Miranda et al. 1998)

occurrence of bidirectional motions due by the baroclinic pressure gradient force at the neighborhood of the u = 0 velocity.

The sub-superficial velocity nucleus of low velocity (0.2 m s^{-1}—Fig. 5.18 upper) during the flood, which is associated with an increase in the halocline stratification (Fig. 5.18 lower), may be due to the low vorticity shear generated by the bottom friction stress. An opposite occurrence (halocline erosion during the tidal ebb) due to the intensification of the vertical mixing is generated by an increase in the bottom stress vorticity as demonstrated by Zhou (1998).

The time mean salinity and the u-velocity profiles for two semidiurnal tidal cycles, calculated by Eqs. (5.19) and (5.20), are presented in Fig. 5.19. These results simulate nearly steady-state conditions and may be used to classify estuaries with the Stratification-circulation Diagram. The salinity profile has an accentuated halocline with values varying from the surface (S_s = 15.84‰) to (S_f = 29.95‰) at the bottom (Fig. 5.19, left), indicating a highly stratified estuary. Its mean depth average is equal to $\overline{S} = 25.8‰$, and the stratification parameter $S_P = \delta S/\overline{S} \approx 0.55$. The u-velocity component, without the influence of the barotropic gradient pressure force indicates a bidirectional motion due to the gravitational circulation (seaward and landward in the upper and lower layer, respectively), which is another characteristic of the partially mixed estuary, with the no-motion depth at $Z \approx -0.5$ ($z \approx 3.0$ m). The velocity values to calculate the circulation parameter u_s = 0.15 m s^{-1} and the residual or net velocity $u_f \approx u_a \approx 0.04$ m s^{-1}. Thus, the circulation parameter, $C_P = u_s/u_f \approx u_s/u_a = 3.7$; finally, with these parameters the investigated estuarine channel can be classified as type 2b. Finally, it should be pointed out that although the low net value of the velocity it is responsible for the seaward advective flux and transport of the concentrations of any property natural or pathogenic.

5.6 Flux and Transport of Properties

The mixing in the estuarine water mass (river + seawater), is physically determined by the local variation of a property concentration ($\partial C/\partial t$) due to the simultaneous action of turbulent diffusion (dispersion) and the advective processes. As the diffusive and the advection are inherent to the motion of non-homogeneous fluids, it is opportune to include in this chapter the fundamental concepts related to the terminologies and determinations of flux and transport of volume and mass (salt), which may also be applied for any conservative property.

Taking into account the physical principles of Hydrodynamics, it is well known that the *volume and mass transport*s of a property is the volume and mass of the fluid flow through a transversal section per unit of time. Then, according to this concept, the *instantaneous* volume transport, $T_V = T_V(t)$, $[T_V] = [L^3T^{-1}]$, and mass $T_M = T_M(t)$, $[T_M] = [MT^{-1}]$, are expressed in volume and mass per time unity. In mathematical terms these quantities are calculated, respectively, by the following surface integrals extended to an area A = A(x, t):

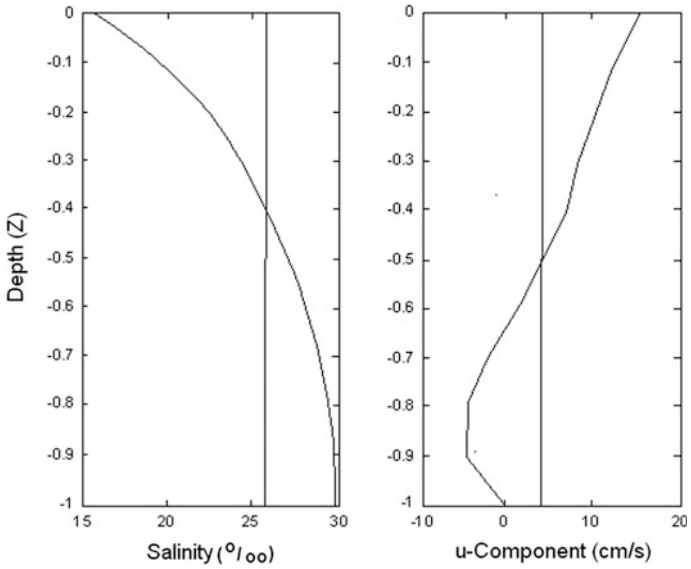

Fig. 5.19 Vertical time mean profiles of salinity and the u-velocity component, determined with hourly values measured during two tidal cycles, sampled during neap tide in the Bertioga estuarine channel (São Paulo, Brazil). The vertical mean depth values of salinity and velocity are shown by *vertical lines* (adapted from Miranda et al. 1998)

$$T_V = \iint_A \vec{v} \cdot \vec{n}\, dA = \iint_A u dA = \overline{u}A, \tag{5.24}$$

and

$$T_M = \iint_A \rho \vec{v} \cdot \vec{n}\, dA = \iint_A \rho u dA = \overline{\rho u}A, \tag{5.25}$$

where the dot, •, indicates the scalar product, and in the last term on the right-hand-side of these equations the *mean value theorem* was used, in Eqs. (5.24) and (5.25), the quantities $\overline{u}$ and $\overline{\rho}$ indicate the mean values of the u-velocity component and density in the area, A, respectively. The transports, T_V and T_M, in the SI system of units are given in $m^3\ s^{-1}$ and $kg\ s^{-1}$, respectively. The same equations are applied for a transverse cross-sectional area, A, in an estuary; however, the experimental fields of velocity $(\vec{v})$ and density, $\rho = \rho(S, T, p)$, may only be measured at discrete points or oceanographic stations, distributed in a cross-section, A, and the area integrals of these equations must be calculated numerically, because the functional relationship $u = u(x, y, z, t)$ are not analytically known. Further details on the transport determination methods will be given later.

The *instantaneous volume transport*, divided by the cross section area (A), is named *volume flux* (ϕ_V), and it is numerically equal to the mean transport at the

transversal section. Then, this physical quantity is calculated by ϕ_V/A, or by combining this definition with Eq. (5.24),

$$\Phi_V = \frac{1}{A}\iint_A \vec{v}\cdot\vec{n}\,dA = \frac{1}{A}\iint_A u dA = \overline{u}. \tag{5.26}$$

Then, the *volume flux* is numerically equal to the mean velocity value in the transversal section A.

By analogy, it is possible to define the *mass flux* ($\phi_M = T_M/A$) from Eq. (5.25),

$$\Phi_M = \frac{1}{A}\iint_A \rho\vec{v}\cdot\vec{n}\,dA = \frac{1}{A}\iint_A \rho u dA = \overline{\rho u}. \tag{5.27}$$

The *salt flux* (Φ_S) may be calculated by inserting the salinity ($S \times 10^{-3}$, converted in kg/kg units) into the integrand of Eq. (5.27). Hence, the salt flux is $\Phi_S = \rho v S \times 10^{-3}$, $[\Phi_S] = [ML^{-2}T]$ which, integrated in the area, A, of the transversal section, results in the salt transport T_S, $[T_S] = [MT^{-1}]$, and in SI unities, this quantity is expressed in kg s^{-1}.

Determinations of volume and mass transport in estuarine studies is always important, particularly when the objectives of the research are to investigate the import or exportation of natural concentrations of biological, chemical substances, suspended sediments, and pathogenic substances. In practice, this determination merits special attention due to the temporal and spatial variability of the evolved properties and the cross-section area (A).

Let us use an example of the determination of the volume transport across a transversal section, with the following data known: the area (A) of transverse section area, and the steady-state velocity field based on measurements at three oceanographic stations A, B, C shown in Fig. 5.20. After the vector velocity decomposition, corresponding to the scalar product $\vec{v}\cdot\vec{n} = u$ (the function being integrated in the first term of Eq. 5.24) with known u-velocity component profiles at stations A, B and C, it is possible to drawn the vertical velocity field u = u(y, z), as illustrated in Fig. 5.20.

Figure shows the occurrence of a bi-directional motion, and, as may be observed in the signal changes of the velocity field, the motion has a layer of null velocity (u = 0). In the assumption that the motion is occurring in an estuarine channel, it is characteristic of a partially-mixed estuary (type 2 or B, according to the classification criteria) in nearly steady-state, with motions down and up estuary in the upper and lower layers, respectively. With the velocity isolines (u = const.) drawn in this figure, it is possible to numerically calculate the volume transport (Eq. 5.24) with the following steps:

(a) With a planimetry technique, the area $[L^2]$ between the velocity isolines may be determined;
(b) The mean value of the area between the isolines is multiplied by the mean velocity value between them $[L^2LT^{-1}]$

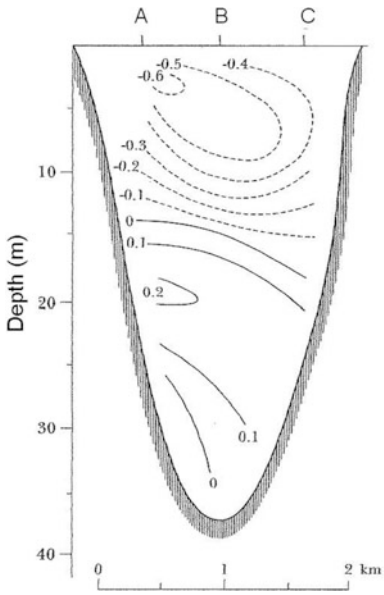

Fig. 5.20 Steady-state vertical structure of the u-velocity component, u = (y, z), in m s^{-1}, orthogonal to the vertical section. *A*, *B*, and *C* are positions of oceanographic stations. The Ox axis is oriented in the landward direction (u > 0 and u < 0) indicate flood and ebb, respectively

(c) The sum of all these numerical value of the integral and the volume transport through the vertical section.

As the velocity is given in m s^{-1} and the area calculated in m^2, the net volume transport is approximately—1.2×10^3 m^3 s^{-1} (-3.2×10^3 m^3 s^{-1} and 2.0×10^3 m^3 s^{-1}, seaward and landward, respectively). The same procedure may be used to calculate the mass and salt transport; however, in these cases, in the transversal section, the isolines of the ρu and ρuS quantities must be drawn, and the mean velocity multiplied by the corresponding isolines values.

Acoustic Doppler Current Profilers (ADCP) may perform velocity profile measurements accurately and at short time intervals along estuarine cross sections, enabling accurate determination of volume transport across transversal sections. The software of the ADCP equipment may also automatically compute the volume transport; however, the displayed results must be checked against other methodologies.

Let's now consider a non-stationary velocity profile, u = u(x, t), in a known fixed position in an estuarine transversal cross section. With this profile, it is possible to calculate its mean velocity value $\overline{u} = \overline{u}(t)$ in the water column, with depth h = h(t), which oscillate periodically with time. With these data it is possible to calculate the volume transport, $(T_V)_L$, per unit of the section width, which is representative of the neighboring geographic position. Then, the net volume transport is given by:

$$\left\langle (T_V)_L \right\rangle = \frac{1}{T}\int_0^{T_P} \overline{u}(t)h(t)dt = \langle \overline{u}h \rangle. \tag{5.28}$$

In this equation T_P is the tidal period, and the volume transport dimension is $[(T_V)_L] = [L^2T^{-1}]$. Under normal meteorological conditions and for a laterally homogenous estuary with a width, B, the product $B\left\langle (T_V)_L \right\rangle$ is the numerical approximation of the fresh water discharge (Q_f) at the estuary head.

Because, in general, the integrand of Eq. (5.28) is not known analytically, this volume transport may be numerically calculated with an equation similar to Eq. (5.20);

$$\left\langle (T_V)_L \right\rangle = \frac{1}{n}\left[\frac{\overline{u}(t_0)h(t_0)}{2} + \sum_k \overline{u}(t_k)h(t_k) + \frac{\overline{u}(t_n)h(t_n)}{2}\right], \tag{5.29}$$

where n is the number of lunar hours of the tidal cycle and k = 1, 2, …, n − 1.

When the functions $\overline{u} = \overline{u}(t)$ and h = h(t) of Eq. (5.28) are known, this equation may be integrated by analytical methods. Under the assumption velocity and level oscillations may be simulated by sinoidal oscillations, similar to the solutions obtained for the propagation of a tidal wave in a channel with infinity length (Eqs. 2.21 and 2.22, Chap. 2),

$$h(t) = H_0 + \eta_0 \sin(\omega t - \Phi), \tag{5.30}$$

and

$$u(t) = u_0 + U_0 \sin(\omega t), \tag{5.31}$$

where the angle, Φ, is the phase difference between the velocity and the water depth variations. In these equations, H_0 and u_0 are the mean sea-level depth and the mean velocity, which are superimposed to the values η_0 and U_0, respectively.

Replacing Eqs. (5.30) and (5.31) in Eq. (5.28), simplifying the resulting expression with trigonometric identities and completing the resulting analytical integration, it follows that the expression for the mean volume transport is,

$$\left\langle (T_V)_L \right\rangle = u_0 H_0 + \frac{U_0 \eta_0}{2}\cos(\Phi), \tag{5.32}$$

This final result indicates the volume transport, per unit of the transversal section, which may be determined only by the product of the mean values (u_0 H_0) when the phase difference is equal to π/2, and the tidal oscillation in the estuarine channel is a stationary wave. This phenomenon has been observed in some estuaries where time differences of (T_P/4) or phase difference of π/2, between the tidal height oscillations and the longitudinal velocity differences were detected (Dyer and Ramamoorthy,

1969; Kjerfve 1970, 1973). However, when the tidal wave propagates as a progressive wave, $\Phi = 0$ (Eq. 2.24, Chap. 2), the volume transport is determined taking into account the tide and velocity amplitudes ($u_o H_o$). In partially stratified estuaries (type 2 or B), the phase differences vary in the interval $0 < \Phi < \pi/2$, and the volume transport also depends on the product $U_0\eta_0$. If the estuary width may be approximated by a constant value (B), the volume transport across the transversal section may be calculated by $B\langle(T_V)_L\rangle$.

5.7 Advective Salt Transport Components

The landward salt transport is driven by the current velocity generated during the tidal flood and gravitational circulation, while the seaward salt transport is driven by the reversal of the tidal oscillation, the ebb tidal current, the fresh water discharge and gravitational circulation. To gain a better understanding of these processes, Pritchard (1954) studied the salinity and current velocity measured in the James river estuary (Virginia, USA), averaged over several tidal cycles. This study confirmed the hypothesis that the mixing processes are related primarily to tidal forcing, and suggested the possibility of predicting the eddy diffusion terms from the tidal velocities. Pritchard (op. cit.) also showed that the horizontal advective flux and the vertical non-advective (diffusive) flux of salt are the most important factors in maintaining the salt balance; however, although the vertical advective flux is of secondary importance but still significant, the longitudinal non-advective (diffusive) salt flux is small. Confirming these results, in studies on the salt dispersion in the Hudson river estuary (New York, USA), Hunkins (1981) stated that at the simplest level, an estuary may be considered as a *black box* which pumps salt upstream against the mean river flow, and the overall landward mixing is better termed dispersion, rather than diffusion, and that dispersion is produced primarily by the effects of winds, tides and gravitational circulation. Thus, the process termed dispersion has advection and vertical turbulent diffusion as main components.

For studies on the advective and non-advective salt transport components through an estuary transverse cross-section, measurements of current velocity and salinity must be taken at Δt intervals from 30 min to 1 h for a duration at least one complete tidal cycle, and the profiles of these properties must be interpolated at the non-dimensional depth (Z). To simplify the mathematical treatment, consider a lateral homogeneous estuary, which is a simplified version of the non-laterally homogeneous estuary studied by Hunkins (1981). Under this simplification, it is assumed that the experimental data are from a single fixed station in the middle of the channel, and the instantaneous salt transport (M_S), per width unit, is determined by:

$$M_S = \int_0^h \rho S\vec{v} \cdot \vec{n}.dz = \int_0^h \rho u S dz = \langle \overline{\rho u S} h \rangle, \tag{5.33}$$

In this equation, the Oz axis is oriented in the $\vec{g}$ direction, and in the last term of this equation $(\overline{\rho u S})$ is the mean value of the flux salt, and h is water thickness. The dimensional analysis of this equation shows that M_S, $[M_S] = [ML^{-1}T^{-1}]$ is calculated in the SI system of units, in kg m^{-1} s^{-1}.

The mean advective salt transport (T_S) during one (T_P) or more tidal cycles (nT_P) is calculated by:

$$T_S = \langle M_S \rangle = \frac{1}{T} \int_0^T M_S dt = \langle \overline{\rho u S} h \rangle. \tag{5.34}$$

The mean density in the water column, appearing in Eqs. (5.33 and 5.34), is calculated by a State Equation of Sea Water, at atmospheric pressure.

The term $\langle \overline{\rho u S} h \rangle$ in Eq. (5.34) is the mean values in space (depth) and time. Considering u-velocity component and salinity as examples, the time mean depth value, are calculated by:

$$\langle \overline{u} \rangle = u_a = \frac{1}{T} [\frac{1}{h} \int_0^h u(x, z, t)] dt, \tag{5.35a}$$

and

$$\langle \overline{S} \rangle = S_a = \frac{1}{T} [\frac{1}{h} \int_0^h S(x, z, t)] dt. \tag{5.35b}$$

These time-mean values are function of the longitudinal distance and its value varies according to the cross-sectional area, and u-velocity component may be considered in first approximation to the velocity component generated by the river discharge,

$$\langle \overline{u} \rangle = u_a \approx \frac{Q_f}{A}. \tag{5.36}$$

As demonstrated in the pioneer article of Bowden (1963), the advective salt transport also has contributions of a diffusive nature that don't explicitly appear in Eq. (5.34). This phenomenon may be investigated with the separation of the periodic tidal forcing (barotropic), the gravitational circulation (baroclinic) and other effects, such as the turbulence generated by the wind. The main objective of

the following theoretical treatment is to separate the longitudinal salt transport in dominant parcels. For this purpose, the longitudinal velocity component (u) the salinity (S) and the water depth (h) must be decomposed in determinate parcels to make identification of the various correlations possible, which indicate the advective and dispersive physical processes responsible for the landward and seaward salt transport. This decomposition process may be used in the determination of the transport components of any conservative substance dissolved in the seawater.

Using the articles of Bowden (1963), Fischer (1976), Hunkins (1981), Dyer (1974) and Kjerfve (1986), as references for a laterally homogenous estuarine channel, the instantaneous velocity and salinity profiles are decomposed into mean, tidal, steady (subscripts a, t, s) and deviation terms (′):

$$u(x,\ z,\ t) = u_a(x) + u_t(x,t) + u_s(x,z) + u'(x,\ z,\ t), \tag{5.37}$$

$$S(x,\ z,\ t) = S_a(x) + S_t(x,\ t) + S_s(x,\ z) + S'(x,\ z,\ t). \tag{5.38}$$

In the decompositions, the first term on the right-hand-side are the mean values $u_a(x) = \langle \overline{u} \rangle$ and $S_a(x) = \langle \overline{S} \rangle$ due to the dominant influence of the river discharge (advective process). The second and third terms of these equations, $u_t(x, t)$, $u_s(x, z)$, $S_t(x, t)$, $S_s(x, z)$, mathematically simulate the cyclic tidal influence and the stationary influence of the gravitational circulation, respectively, which also are dominant. These components are defined as,

$$u_t = \overline{u} - u_a, \tag{5.39}$$

$$S_t = \overline{S} - S_a, \tag{5.40}$$

$$u_s = \langle u \rangle - u_a \tag{5.41}$$

$$S_s = \langle S \rangle - S_a, \tag{5.42}$$

where the expressions (5.39 and 5.40) and (5.41 and 5.42) are the tidal and the steady-state components, respectively. The last terms, $u'(x, z, t)$ and $S'(x, z, t)$, of Eqs. (5.37) and (5.38) are the deviation components due to the dispersive small scale physical processes, and are calculated by,

$$u' = u(x,z,t) - u_t(x,t) - u_s(x,z) - u_a(x), \tag{5.43}$$

and

$$S' = S(x,z,t) - S_t(x,t) - S_s(x,z) - S_a(x). \tag{5.44}$$

Figure 5.21 shows the velocity decomposition in the parcels u_t, u_s and u' from the vertical profiles; profile (a) the nearly steady-state profile (averaged during one or more tidal cycles) and, (b) the instantaneous profile. The same schematic profiles may be used for the salinity components (S_t, S_s and S').

As the water column thickness varies with the tidal oscillation it must be separated into the following components,

$$h(x,t) = h_a + h_t(x,t), \tag{5.45}$$

where $h_a = \langle h \rangle = H_0$ is the time mean value of the local depth, and $h_t(x, t) = \eta(x, t)$ is the tidal height.

Replacing the decompositions of Eqs. (5.37), (5.38) and (5.45) in Eq. (5.34), the salt transport T_S, $[T_S] = [ML^{-1}T^{-1}]$ will be decomposed into 32 terms. Disregarding the small terms and others without well-defined physical meaning, results in only seven terms to calculate the time mean salt transport (per unity width) during one or more tidal cycles, described by the equation:

$$\begin{aligned} T_S = &\overline{\rho}.(u_a.h_a.S_a + \langle u_t.h_t \rangle S_a + \langle u_t.S_t \rangle h_a + h_a.\overline{u_s.S_s} \\ &+ h_a\left\langle \overline{u'.S'} \right\rangle + \langle u_t.S_t.h_t \rangle + u_a.\langle S_t.h_t \rangle), \end{aligned} \tag{5.46}$$

or

$$T_S = A + B + C + D + E + F + G. \tag{5.47}$$

The terms A–G are related to the processes responsible for the time-mean salt transport or net salt transport.

The first term (A) represents the seaward advection of salt by the mean u-velocity component. The term B is the salt transport generated by the tidal wave propagation in the estuary, due to the inclined topography of the estuarine channel. According to the pioneer article by G.G. Stokes, published in 1847, the orientation of this wave transport is opposite to its propagation, which is known as the Stokes drift phenomenon (Longuett-Higgins 1969). Thus, its contribution to the salt transport is generally seaward, and, like the term A, it constitutes an advective contribution to the salt transport which may be important in macro-tidal estuaries.

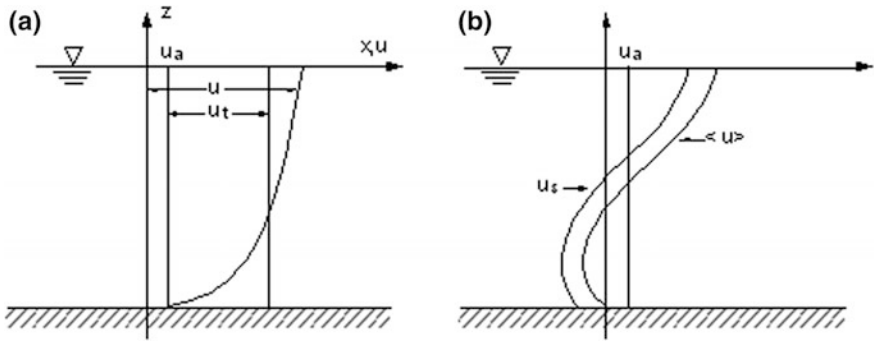

Fig. 5.21 Vertical velocity profiles: the instantaneous (**a**) and time-mean values (**b**), showing the decompositions in the parcels $u_t = \overline{u} - u_a$ and $u_s = \langle u \rangle - u_a$ s(according to Fischer et al. 1979)

The advective processes, A and B, tend to sweep the estuary clear of salt and sharpen the frontal gradient between the river and ocean (Hunkins 1981).

The remaining terms (C–G) are generally considered to represent up-estuary dispersion of salt through mixing of various processes. For the physical interpretation and the orientation (up or down estuary) of these terms, it will be necessary to anticipate the laterally integrated salt conservation equation from Chap. 7 (Eq. 7.80). This equation may be further simplified: with constant width (B = const.), steady-state conditions and vertical velocity component equal to zero (w = 0), because only the longitudinal salt transport is being calculated. In these conditions, the salt balance (advective salt flux = diffusive salt flux) is expressed by,

$$\rho u S = \rho K_E \frac{\partial S}{\partial x}, \tag{5.48}$$

where $u = u_a + U_s$; U_s is the Stokes velocity and K_E is the kinematic dispersive longitudinal coefficient of salt. If all members of this equation are multiplied by the water layer thickness (h), the first member of this equation is the advective salt transport per width unit [$ML^{-1}T^{-1}$], generated by the river discharge and the Stokes drift (terms A + B). Then, this advective salt transport is in balance with the up-estuary salt transport generated by others mechanisms, because under steady-state conditions there is no net transport of salt. Hence, from Eqs. (5.47) and (5.48) it follows (Fischer et al. 1976):

$$-K_E \frac{\partial S}{\partial x} = C + D + E + F + G. \tag{5.49}$$

The terms in the second member of this equation are forced by the combined influences of the tidal stirring and vertical turbulent fluctuations, which have been defined as dispersive mechanisms.

Some of the suggested physical mechanisms connected with the terms of Eq. (5.46) were obtained by Hunkins (1981), through analysis of current and salinity observations in the lower Hudson estuary (New York, USA), providing a basis for assessing the relative importance of the following physical processes:

(i) (A) and (B) total discharge and Stokes wave transport, which have the fresh water discharge as a physical process;
(ii) (C) tidal correlation, with topographic trapping as a physical process;
(iii) (D + E) steady shear dispersion due to the gravitational circulation, bathymetric tidal pumping and steady wind effect;
(iv) (F + G) oscillatory dispersion due to tidal shear and unsteady wind.

The sum A + B is positive and represents the advective salt transport by river discharge. In the case of a standing wave, tidal height and tidal velocity would be 90° out of phase, and the contribution of the term B, which is averaged over the tidal cycle, would vanish. In a long progressive wave, high water occurs at maximum flood and low water at maximum ebb, therefore water is carried up the

estuary along with and its up-estuary salt content, and this term has a negative contribution. However, term A incorporates a compensation current which offsets the landward transport by term B.

The term defined as *tidal correlation* (C), is determined by the mean correlation of the product of velocity (u_t) and salt (S_t) multiplied by h_a, which may be positive, indicating a process that acts to carry salt out of the estuary, such as in the Hudson estuary. In an idealized well-mixed estuary, maximum salinity would be reached at the end of the flood tide, so there will be a phase difference of 90° between u_t and S_t with no net contribution from this term since the integral of these terms in quadrature would be zero. It has been suggested by Fischer et al. (1979) that the trapping of water by topographic irregularities (topographic trapping) along the edge of an estuary with its later release during a different tidal stage, could lead to a phase difference of less than 90°. This would be a dispersive process, leading to a negative value for term C. It is generally observed in partially mixed estuaries that the longitudinal salinity gradients are less in the lower layer than they are in the upper layer; consequently, the tidal salinity oscillation is substantially reduced in the lower layer. Also, the tidal current near the bottom affects the tidal current in the upper layer due to the frictional effects. Due to these two well documented characteristics of estuarine circulation, the tidal salinity must lag behind the tidal current by a phase angle greater than 90°, which makes the term C positive.

The component D, defined as *steady shear dispersion*, is due to the vertical gravitational circulation minus the circulation generated by the river discharge. As it acts up-estuary it is not only the largest contribution to the salt dispersion but is also subjected to the largest fortnightly and seasonal changes in partially stratified estuaries. It has a small contribution in well-mixed estuaries. The component E results from the oscillatory turbulent shear with a time scale less than the tidal oscillation generated by the wind; it usually has a small contribution to the salt balance.

The oscillatory dispersion components (F and G) were investigated by Hunkins (1981) and Kjerfve (1986) and have tidal shear and unsteady wind effect as physical processes. They were introduced in the decomposition of the advective salt transport because they may be important in well-mixed estuaries forced by mesotides. The component F, calculated by the triple correlation of the temporal variations of the u-velocity component (u_t), salinity (S_t) and tide (h_t), is by definition the *oscillatory dispersion*. In the component G, the mean value of salinity (S_t) and tidal height (h_t) correlations are multiplied by the river discharge velocity (u_a) and is, in general, dispersive and named oscillatory dispersion. The lack of consistency of its determinations in the Hudson estuary suggests that they were too small to be adequately sampled.

Equations (5.34) and (5.46) are different mathematic expressions of the same physical quantity, the salt transport. Consequently, the comparison of their results may be used to verify the computational results, and also to indicate that the neglected terms in Eq. (5.46) are negligible.

Although there are difficulties in identifying reliable measurements for the application of this method for the decomposition of the advective salt transport, it has

been used in studies related to the contribution of various mechanisms in estuaries with different salinity stratifications (Bowden 1963; Dyer 1974; Hunkins 1981; Lewis and Lewis 1983; Kjerfve 1986, and others). As an example of this method applied to a partially mixed estuary (type 2b or B), Table 5.2 presents the results obtained from measurements made in the Bertioga estuarine channel (Fig. 1.5, Chap. 1) during neap tide.

In this experiment, the salt transport was dominated by the advective component (A) and the shear dispersion component (D), generated by the gravitational circulation. In a steady-state condition, the salt transport (T_S) should converge to zero. In this example, $T_S \neq 0$, due to seaward net salt transport equal to 3.54 kg m^{-1} s^{-1}, calculated by the sum of all individual terms; almost the same value (3.61 kg m^{-1} s^{-1}) was obtained applying Eq. (5.34), which confirms the results of the individual terms.

Among the advective salt transport components in the entrance channel of the Patos lagoon, which were calculated from the same data set that was used to classify the estuary as well-mixed (type 1b), the following components were predominant: the advective term A due to the fresh water discharge, and the oscillatory dispersion terms (F + G) generated by the up-lagoon salt transport forced by a meteorological frontal zone (Möller and Castaing 1999).

In laterally non-homogeneous estuaries it is necessary to include the cross-section variations, A = a(x, t), due to the tidal height oscillation, which is decomposed into two components, $A(x, t) = \langle A \rangle + A_t(x, t)$, a time mean area and its time variation, respectively, to take into account its transverse variation. This procedure will increase the complexity of the mathematical treatment and, for further details on this subject, we recommend the Hunkins (1981) article, where advective and dispersive components of salt transport were calculated in transversal sections of the Hudson estuary (New York, USA).

Table 5.2 Advective salt transport components (in kg m^{-1} s^{-1}) for an experiment with hourly measurements during two neap tidal cycles in the Bertioga estuarine channel (SP) (according to Miranda et al. 1998)

Definition	Physical process	Formulation	Transport
A-Total discharge	Fresh water discharge	$\overline{\rho}.u_a.h_a.S_a$	5.97
B-Stokes wave transport	Fresh water discharge	$\overline{\rho}.\langle u_t.h_t \rangle S_a$	−0.16
C-Tidal correlation	Topographic trapping	$\overline{\rho}.h_a\langle u_t.S_t \rangle$	−0.49
D-Steady shear dispersion	Gravitational circulation	$\overline{\rho}.h_a.\overline{u_s S_s}$	−1.32
E-Steady shear dispersion	Bathymetry, tidal pumping, steady wind effects	$\overline{\rho} h_a \langle \overline{u' S'} \rangle$	−0.45
F-Oscillatory dispersion	Tidal shear	$\overline{\rho}\langle u_t.S_t.h_t \rangle$	−0.04
G-Oscillatory dispersion	Unsteady wind effect	$\overline{\rho}.u_a\langle S_t.h_t \rangle$	0.03
T_S = A + B + C + D + F + G			3.54
T_S (Eq. 5.34)			3.61

5.8 Advective Concentration Transport

One of the objectives for measuring velocity, salinity and temperature in estuaries is to use these properties to calculate the flux and transport concentrations of these properties. In this case, let us consider a conservative substance concentration (C), which has been simultaneously measured with the hydrographic properties and current velocity. As this property may be determined by the ratio of its mass or volume per unit of mass, its dimensions are $[C] = [MM^{-1}]$ or $[L^3M^{-1}]$, these concentrations must be taken into account in the determinations of the corresponding flux or transport.

For instance, if C is the oxygen concentration dissolved in the estuarine water mass, which being a non-dimensional property, is usually determined volume of oxygen per volume $[L^3L^{-3}]$. Then, the mathematical expression to calculate the time mean flux (Φ_{O_2}) across an area, A, during the tidal cycle is determined by:

$$\Phi_{O_2} = \frac{1}{T}\int_0^T \left[\frac{1}{A}\iint_A (C\vec{v}\cdot\vec{n}dA)\right]dt = \langle\overline{cu}\rangle. \tag{5.50}$$

From this equation, it follows that Φ_{O_2} has dimension of $[L^3L^{-2}T^{-1}] = [LT^{-1}]$. This result represents the physical dissolved oxygen volume contents crossing the unity of the transversal section per time unity (oxygen flux). If in Eq. (5.50) the factor (1/A) is eliminated, the result is the oxygen transport, T_{O_2} (volume per time unity, and $[T_{O_2}] = [L^3T^{-1}]$).

Under the assumption that the concentration, C, of a given property is now expressed as a generic property (Pr) per mass unity $[PrM^{-1}]$, then its flux Φ_C is calculated by,

$$\Phi_C = \frac{\overline{\rho}}{T}\int_0^T \left[\frac{1}{A}\iint_A (C\vec{v}\cdot\vec{n}dA)\right]dt = \overline{\rho}\langle\overline{cu}\rangle, \tag{5.51}$$

where the flux Φ_C and its dimension is expressed by $[\Phi_C] = [PrL^{-2}T^{-1}]$. If the factor (1/A) is eliminate from this equation, the result is property transport (property per time unity, in dimension $[PrT^{-1}]$.

Equations (5.50 and 5.51) may also be used to calculate the flux or transport of any property if the measured concentration is expressed as the salinity unity, which is non-dimensional. Equations (5.34) and (5.51) are similar, and the only difference is that the first equation gives salt transport per unit of the transversal section. Then, it is always possible, with the same treatment as described in the previous topic (5.7), to perform decomposition of the property transport into advective and dispersive components and investigate the main mechanisms and physical processes responsible for the exportation or importation of substances in estuaries.

River discharge and Stokes drift are exportation mechanisms which decrease the concentrations of harmful substances introduced into rivers of directly into estuaries. Due to the potential danger to the estuarine environment, the monitoring of harmful substances is of fundamental importance to estuary management, because estuaries' natural conditions may be drastically altered by construction of sand bars, navigational channels, river diversion and fresh water used for urban, agriculture and industrial purposes.

The main methods of reduction, and processing hydrographic and velocity data presented in this chapter have their algorithms programmed in the computational environment MatLab®, described in Bergamo et al. (2002).

5.9 Tidal Prism Determination

When the u-velocity component, u = u(y, z, t), as presented in Fig. 5.20, is measured at regular time intervals in a transversal section at the estuary mouth from the low tide (t = 0) to the high tide (t = $T_P/2$), it is possible to determine the tidal prism T_{PR}, defined in Chap. 2, by the following mathematical expression:

$$T_{PR} = \int_0^{T_P/2} \left[\iint_A u(y, z, t) dA \right] dt. \tag{5.52}$$

In this equation the surface integral over the area A (whose numerical integration has been described), is the volume transport [L^3T^{-1}]. The integration in the time domain between the time interval [0—$T_P/2$] may also be determined numerically using an algorithm similar to those presented in Eq. (5.20). This integration (Eq. 5.52) may also be to calculate automatically with an Acoustic Doppler Current Profiler (ADCP), performing velocity profile measurements accurately and at short time intervals, but these results must be checked against others methodologies.

References

Bendat, J. S. & Piersol, A. G. 1966. Measurement and Analysis of Random Data. New York, Wiley. 390 p.

Bérgamo, A. L.; Miranda, L. B. de & Corrêa, M. A. 2002. Estuário: Programas para Processamento e Análise de Dados Hidrográficos e Correntográficos. Rel. Téc. Instituto Oceanográfico, São Paulo, (49):1–16.

Blumberg, A. F. 1975. A Numerical Investigation into the Dynamics of Estuarine Circulation. Tech. Rept. Chesapeake Bay Institute, The Jonhs Hopkins University. n. 91. 110 p. + Apêndices.

Bowden, K. F. 1963. The Mixing Processes in a Tidal Estuary. J. Air Wat. Pollut., 7:343–356.

Bowden, K. F. 1978. “Mixing Processes in Estuaries”. In: Kjerfve, B. (ed.). Estuarine Transport Processes. University of South Carolina Press, Columbia, pp. 11–36. (Belle W Baruch Library in Marine. Science, 7).

Chriss, T. M. & Caldwell, D. R. 1984. Universal Similarity and Thickness of the Viscous Sublayer at the Ocean Floor. J. Geophys. Res., 89(C4):6403–6414.

Csanady, G. T. 1982. Circulation in the Coastal Ocean. D. Reidel Publishing, Dordrecht, 279 p. (Environmental Fluid Mechanics).

Defant, A. 1961. Physical Oceanography. Oxford, Pergamon Press, vol. 1. 729 p.

Dyer, K. R. 1974. The Salt Balance in Stratified Estuaries. Estuar. Coast. Mar. Sci., 2:273–281.

Dyer, K. R. 1977. Lateral Circulation Effects in Estuaries. Estuaries, Geophysics and the Environment. Washington, D. C., National Academy of Sciences, pp. 22–29.

Dyer, K. R. 1986. Coastal and Estuarine Sediment Dynamics. New York, Wiley. 342 p.

Dyer, K. R. & Ramamoorthy, K. 1969. Salinity and Water Circulation in the Vellar Estuary. Limnol. Oceanogr., 14(1):4–15.

Elliott, A. J. 1976. A Study of the Effect of Meteorological Forcing on the Circulation in the Potomac Estuary. Spec. Rept. n. 56, reference 76-9, Chesapeake Bay Institute, The Johns Hopkins University, 67 p.

Fischer, H. B. 1976. Mixing and Dispersion in Estuaries. Ann. Rev. Fluid Mech., 8:107–133.

Fisher, J. S.; Ditmars, J. D. & Ippen, A. T. 1972. Mathematical Simulation of Tidal Time Averages of Salinity and Velocity Profiles in Estuaries. Massachusetts Institute of Technology, Mass., Rept. MITSG 72–11, 157 p.

Fischer, H. B.; List, E. J.; Koh, R. C. Y.; Imberger, J. & Brooks, N. H. 1979. Mixing in Inland and Coastal Waters. New York, Academic Press. 483 p.

Geyer, W. R. 1997. Influence of Wind on Dynamics and Flushing of Shallow Estuaries. Estuar. Coast. Shelf Sci., 44:713–722.

Hanselman, D. & Littlefield, B. 1998. Mastering MatLab 5. A comprehensive Tutorial and Reference. Prentice Hall, The MatLab® Curriculum Series, 638 p.

Heathershaw, A. D. 1981. Comparisons of measured and predict sediment transport rates in tidal currents. Mar. Geol., 42:75–104.

Hunt, J. N. 1964. Tidal Oscillations in Estuaries. Geophys. J. R. Astr. Soc., 8:440–455.

Hunkins, K. 1981. Salt Dispersion in the Hudson Estuary. J. Phys. Oceanogr., 11:729–738

Ianniello, J. P. 1977. Tidally induced residual currents in estuaries of constant breadth and depth. Journal of Marine Research, 35(4), 755–786.

Jay, D. A. & Musiak, J. D. 1996. Internal Tidal Asymmetry in Channel Flows: Origins and Consequences. In: Pattiaratchi C. ed. Coastal and Estuarine: Mixing in Estuaries and Coastal Seas. American Geophysical Union, pp. 211–249

Jenkins, G. M. & Watts, D. G. 1968. Spectral Analysis and its Application. San Francisco, Holden-Day. 525 p.

Kjerfve, B. 1970. Description of a Georgia Estuary. M. S. Essay. Seattle, Dept. of Oceanography, University of Washington. 43 p.

Kjerfve, B. 1973. Volume Transport, Salinity Distribution and Net Circulation in Duplin Estuary. Tech. Rept. ERC 0273. Marine Institute, Georgia, University of Georgia, 30 p.

Kjerfve, B. 1975. Velocity Averaging in Estuaries Characterized by a Large Tidal Range to Depth Ratio. Estuar. Coast. Mar. Sci., 3:311–323.

Kjerfve, B. 1986. Circulation and Salt Flux in a Well Mixed Estuary. In: Van de Kreeke, J. (ed.). Physics of Shallow Estuaries and Bays. Berlin, Spring-Verlag, pp. 22–29.

Lesht, B. M. 1979. Relationships between sediment resuspension and the statistical frequency distribution at bottom shear stress. Mar. Geol.:M19–M27.

Lewis, R. E. & Lewis, J. O. 1983. The Principal Factors Contributing to the Flux of Salt in a Narrow, Partially Stratified Estuary. Estuar. Coast. Mar. Sci., 16:599–626.

Longuet-Higgins, M. S. 1969. On the Transport of Mass by Time-Varying Ocean Currents. Deep-Sea Res., 16:431–447.

Lueck, R. G. & Lu, Y. 1997. The Logarithmic Layer in a Tidal Channel. Continent. Shelf Res., 17 (14):1785–1801.

McAlister, W. B.; Rattray Jr, M. & Barnes, C. A. 1959. The Dynamics of a Fjord Estuary: Silver Bay, Alaska. Department of Oceanography. Tech. Rept. n. 62, University of Seattle, WA.

Merz, A. 1921. Die Strömungen von Bosphorus un Dardanellen. Verh. d. 20. Dtsch. Geogr.-Tag Juni, 1921.

Miranda, L. B.; Castro, B. M. de. & Kjerfve, B. 1998. Circulation and Mixing in the Bertioga Channel (SP, Brazil) Due to Tidal Forcing. Estuaries, 21(2):204–214.

Möller, O. O. Jr., 1996. & Castaing, P. 1999. Hydrographical Characteristics of the Estuarine Area of Patos Lagoon (30°S, Brazil). In: Perillo G. M. E; Picollo, M. C. & Pino-Quivira M. (eds.). Estuaries of South America: Their Geomorphology and Dynamics. Berlin, Springer-Verlag, pp. 83–100 (Environmental Science).

Morettin, P. A. 1999. Ondas e Ondaletas: Da Análise de Fourrier à Análise de Ondaletas. Edusp, São Paulo. 272 p. (Acadêmica 23).

Mossby, H. 1947. Experiments of turbulence and friction near the bottom of the sea. Bergens Mus. Aarb. 1946/1947, Naturv. Rek. No. 3, Bergen, 1947.

Pennington, R. H. 1970. Computer Methods and Numerical Analysis. 2. ed., Macmillan. 452 p.

Pritchard, D. W. 1954. A Study of Salt Balance in a Coastal Plain Estuary. J. Mar. Res., 13 (1):133–144.

Rayner, J. N. 1971. An Introduction to Spectral Analysis. London, Pion. 174 p. (Monographs in Spatial and Environmental Systems Analysis, 2).

Simpson, J. H.; Brown, J.; Mattews, J. & Allen, G. 1990. Tidal Straining, Density Currents, and Stirring in the Control of Estuarine Stratification. Estuaries, 13(2), p. 125–132.

Soulsby, R. L. 1983. The Bottom Boundary Layer of Shelf Seas. In: Johns B. (ed.). Physical Oceanography of Coastal and Shelf Seas. Amsterdam, Elsevier, pp. 189–266. (Oceanography Series, 35).

Sternberg, R. W. 1968. Friction Factors in Tidal Channels with Differing Bed Roughness. J. Mar. Geol., 6:243–260.

Sverdrup, H. U.; Johnson, M. W. & Fleming, R. H. 1942. The Oceans, their Physics, Chemistry and General Biology. New Jersey, Prentice-Hall. 1042 p.

Valle-Levinson, A.; Miller, J. L. & Wheless, G. H. 1998. Enhanced Stratification in the Lower Chesapeake Bay Following Northeasterly Winds. Continent. Shelf Res., 18:1631–1647.

Weisberg, R. H. 1976. A Note on Estuarine Mean Flow Estimation. J. Mar. Res., 34(3):387–394.

Zhou, M. 1998. Influence of Bottom Stress on the Two-layer Flow Induced by Gravity Currents in Estuaries. Estuar. Coast. Shelf Sci., 46:811–825.